EVOLUTION OF ARCTIC CONTINENTAL SHELVES: MODELLING MORPHODYNAMIC FEEDBACKS TO CLIMATE-DRIVEN INCREASES IN SEA STATES

John G. Malito

A thesis submitted to the faculty of the University of North Carolina at Chapel Hill in partial fulfillment of the requirements for the degree of Master of Sciences in the Department of Marine Sciences.

Chapel Hill
2021

Approved By:

Emily Eidam

Antonio Rodriguez

Brent McKee

Antonia Sebastian

ABSTRACT

John G. Malito: Evolution of Arctic continental shelves: modelling morphodynamic feedbacks to climate-driven increases in sea states
(Under the direction of Emily Eidam)

Arctic continental shelves, including the Alaskan Beaufort Shelf (ABS), are experiencing declines in sea ice coverage and duration which are leading to increasingly energetic sea states and coastal erosion. A Delft3D sediment transport model was developed to test how present-day and projected future waves impact shelf evolution, and how shelf geometry modifies propagation of waves toward the coast. Wave-induced sediment transport and morphologic adjustment were enhanced on a relatively steep ABS shelf section (slope 0.0008) under increased projected waves. Redistribution of sediments from the inner shelf to the middle shelf led to attenuation of projected waves as the shelf evolved, creating a regulatory feedback loop. In contrast, effective wave attenuation across a relatively flat shelf section (slope 0.0003) limited cross-shelf transport and morphologic change. Our findings suggest that morphodynamic feedbacks to the growing Arctic wave climate depend on shelf geometry and can impact future coastal erosion.

To all who helped along the way.

Thank you!

ACKNOWLEDGEMENTS

I sincerely thank my advisor Emily Eidam for providing wisdom on how to apply the sediment transport model to a dynamic Arctic marine environment, and Jaap Nienhuis for his patience and enthusiasm when helping me construct the sediment transport model. I thank David Mohrig for his kindness and optimism in my academic career. I thank my friends, family, and colleagues in North Carolina, Texas, and beyond for their countless contributions to my academic success and mental health. Many fun and fulfilling adventures were had in the completion of this masters degree and Arctic research! The project was funded by the US National Science Foundation (1913195).

TABLE OF CONTENTS

LIST OF TABLES

LIST OF FIGURES

LIST OF ABBREVIATIONS

ABS	Alaskan Beaufort Shelf
AK	Alaska
BCG	Bed Composition Generation
BSS	Brier Skill Score index
CFL	Courant-Friedrichs-Lewey number
CMIP5	Coupled Model Intercomparison Project Phase 5
ERA5	European Centre for Medium-Range Weather Forecasts Reanalysis Version 5
IBCAO	International Bathymetric Chart of the Arctic Ocean
MF	Morphodynamic scaling factor
RCP	Representative Concentration Pathway

CHAPTER 1: EVOLUTION OF ARCTIC SHELVES

1.1 Introduction

Arctic air temperatures are increasing at rates over twice that of the Northern Hemisphere average (Box et al., 2019). Because of climate-driven environmental changes, the Arctic is experiencing rapid declines in sea ice extent (Barnhart et al., 2016), widespread permafrost melt (Obu et al., 2016), accelerated coastal erosion (Gibbs et al., 2017), and coastal flooding (Arp et al., 2010). Furthermore, sea states in the Arctic have been increasing as a function of sea ice decline (Thomson et al., 2016, Casas-Prat & Wang 2020a, Wang et al., 2015). As a result, Arctic coastal communities, infrastructure, and ecosystems are increasingly vulnerable to environmental hazards (Manrique et al., 2018). Effects of climate change on Arctic coastal dynamics remain poorly understood, particularly the feedbacks between continental shelf sediment dynamics and sea states that impact vulnerability at long (centennial to millennial) timescales.

The impact of wave events on Arctic coastal erosion has been well documented (Sturtevant et al., 2004; Barnhart et al., 2014; Arp et al., 2010), but the coupling between long-term Arctic shelf evolution and wave transformation beyond the shoreline is seldom addressed. Waves are transformed as they propagate across a shelf, undergoing refraction, shoaling, diffraction, and dissipation before reaching the coast (Ardhuin et al., 2013; Blanco-Chao et al., 2019; MacVean et al., 2016) and wave energy is presently a key erosive mechanism during the open-water season along Arctic coastlines, together with thermal erosion of ice-rich coastal bluffs (Héquette & Hill, 1993; Hill et al., 1991). The geometry of the cross-shelf profile exerts a control on wave transformation through bottom friction (Dean & Dalrymple, 2004), attenuating waves across the shelf. However, shelf morphology is dictated largely by cross-shelf gradients in wave-induced bed stresses leading to sediment transport and adjustment of the shelf profile shape (Harris & Wiberg, 2002). The result is a feedback between hydrodynamic forcings and sediment transport that determines the shape and stability of the shelf profile over long timescales, a process referred to as morphodynamic equilibrium (Overeem & Fagherazzi 2007; Friedrichs & Wright, 2004).

Adjustments to Arctic shelf morphology can play an important role in determining how the climate-driven growth in sea states may translate to an increase in wave energy at the shoreline, with implications for coastal

erosion. In this study we evaluate the potential morphologic response of ABS shelf profiles to an increased wave climate, and how wave attenuation can impact sediment transport on shelves of different geometries. Since the attenuation of waves across the shelf profile can impact the potential for wave-induced sediment transport and erosion at the coast, we explore the character of waves delivered to the inner shelf after transformation across the middle and outer shelf. We focus the present study on the Alaskan Beaufort Shelf (ABS), as this shelf section can serve as an analog for the Arctic marine environments undergoing these climate-driven changes.

We developed a cross-shelf sediment transport model using Delft3D-FLOW to explore the long-term evolution of the ABS under present and project wave climates, with emphasis on the coupling between hydrodynamic forcings, cross-shelf sediment transport, and morphologic adjustment of the shelf profile. Evolution of two bathymetric transects from different parts of the ABS were evaluated over 1000 years given a present-day wave climate and a projected wave climate modelled under the Representative Concentration Pathway 8.5 forcing scenario for climate change (hereafter referred to as RCP8.5 waves). The millennial time-scale allowed for morphodynamic processes to stabilize after the application of waves and lead to the establishment of equilibrium shelf profiles.

Morphologic change on wave-dominated shelves is determined by the cumulative sum of sediment transport by storm waves balanced by partial recovery during fair-weather periods (Anderson et al., 2010; Ogston & Sternberg, 1999), and wave events are important drivers of sediment transport on the ABS (Hill et al., 1991; Sturtevant et al., 2004). Though it is somewhat unclear whether Arctic storms have been observed to increase in duration and intensity (Day et al., 2018; Sepp & Jaagus 2011; Kistler et al., 2001), delayed freeze-up has caused the open-water season to coincide with the already stormy months of October and November (Thomson et al., 2016). Given the importance of storm waves on the evolution of Arctic shelves, a representative storm was applied to the modelled shelf profiles to investigate the coupling between shelf geometry and the potential for wave-driven sediment transport.

1.2 Background

1.2.1 Alaskan Beaufort Shelf

The Alaskan Beaufort Shelf (ABS) spans 600 km of the northern Alaskan coast, between Point Barrow and the Canadian border (Fig. 1.1). With shelf widths ranging from 50 to 100 km, the ABS is narrow relative to the average Arctic shelf width of 104 km (Norton & Weller, 1984; Harris & Macmillan-Lawler, 2016). Typical

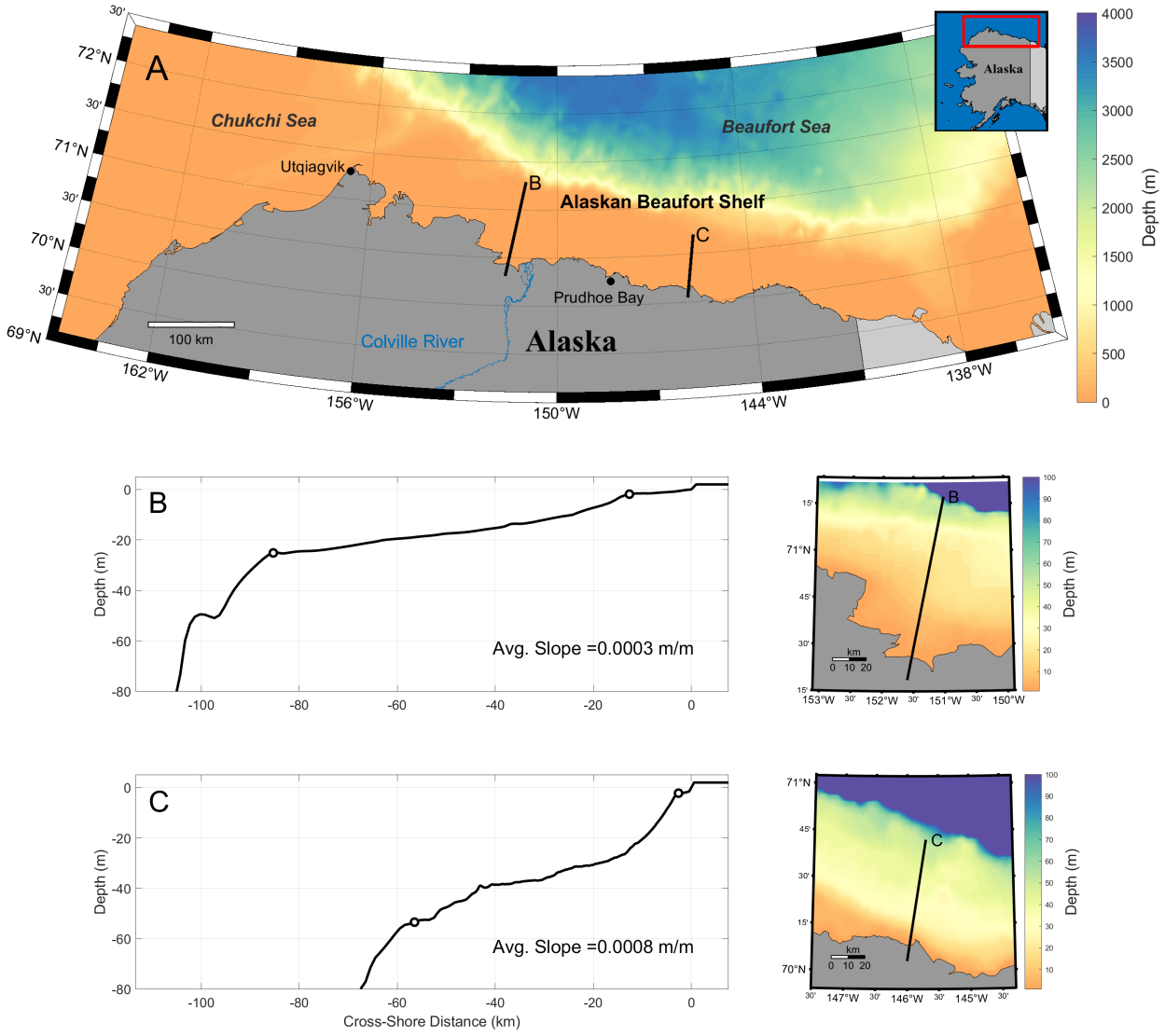

Figure 1.1: (A) An overview of the focus area of this study, the Alaskan Beaufort Shelf, featuring the two cross-shelf transects with contrasting profile slopes, near Harrison Bay (B) and the Flaxman Islands (C). Average transect slope is calculated between the two white circles.

slopes of the ABS fall at or below the global average of 1.8 x 10^{-3}. Therefore, the ABS can be considered an "intermediate shelf" based on global average slopes and widths (Harris et al., 2014). Breaks in shelf slope can occur at various isobaths as a function of sea ice zonation (Reimnitz et al., 1978). A shallow bathymetric platform, or "bench," is common inshore of the 2 m isobath and is likely related to deposition promoted by shorefast ice (Reimntiz et al., 1985) or submerged coastal lagoons (Gibbs et al., 2017). The present shoreline position and shelf morphology were set by 140 m of sea level rise during the Holocene (Hill & Héquette, 1995; Hill et al., 1985). Sea level rise rates on the ABS are approximately 3.5$\pm$1 mm/yr (Manson & Solomon, 2007).

Sediments on the ABS are dominated by fine-grained sand and mud, but size distributions are highly variable (Harper et al., 1990; Fischbein et al., 1987). Distributions of gravels, sands, silts, and clays are patchy (Barnes et al., 1980) due to processes unique to the Arctic such as ice gouging, strudel scour, ice rafted debris, and local currents focused under the cover of ice, all of which expose and transport sediments that were deposited under a different hydrodynamic regime (Barnes & Rearic, 1985; Barnes et al., 1980).

In contrast to temperate and tropical shelves, the ABS is sheltered by sea ice between October and June, leaving a brief window of time in which open-water sediment-transport processes can occur. Increasing wave energy throughout the summer and storms in the fall can generate high bed stresses, storm surge, and changes in near-bed currents (Barnhart et al., 2014; Pickart et al., 2009). Storms most frequently occur between August and October (Hudak & Young 2002; Zhang et al., 2004). Two types of storm systems dominate this region: those originating in the Arctic which bring westerly winds, and those originating in the Gulf of Alaska which bring easterly winds (Lynch et al., 2004; Pickart et al 2013; Forest et al., 2016). Arctic-born storms approaching the ABS from the northwest are the principal drivers of sediment transport during open-water season, generating coastal setup and exposing the coastline to intense wave action (Héquette & Hill., 1993; Manson & Solomon 2007). In fair weather conditions, winds blow predominantly from the east with speeds $<$6 m/s and do not develop significant coastal setdown or wave action (Héquette & Hill, 1993). Though climate-driven changes to storm dynamics remain uncertain (Day et al., 2018), the expanding duration of the open-water season can expose the shoreline to more storms per year. Since storms play a large role in coastal erosion, increased exposure to storm energy could lead to greater retreat rates (Gibbs et al., 2015; Barnhart et al., 2014; Obu et al., 2016; Lynch et al., 2004).

Currents on the shelf are principally shore-parallel and closely coupled to an evenly distributed bimodal wind climate during the open-water season (Forest et al., 2016; Weingartner et al., 2009; Barnes, 1982). Along-shelf currents on the ABS can exceed 20 cm/s during the open-water season and 10 cm/s during periods of ice cover,

but long-term averages are typically near zero due to the bimodal wind climate (Weingartner et al., 2009). Cross-shelf currents are typically <3 cm/s (Weingartner et al., 2017), but are capable of exporting sediments suspended by wave action from the coast via advection during storm events (Héquette & Hill, 1993; Héquette et al., 2001). Furthermore, downslope diffusion of sediments transported by shore-parallel currents may contribute to cross-shelf sediment transport (Hill et al., 1991). The shelf is microtidal (Okkonen, 2016), and tides do not play a significant role in sediment transport on the shelf (Weingartner et al., 2009).

The two principal sources of sediments to the ABS are riverine sediments supplied by the Colville River and eroded coastal sediments which are thought to contribute between 7 to 10 times more sediments than delivered by the Colville River (Rachold et al., 2000; Reimnitz et al., 1988). Much of the ABS coastline consists of ice-rich bluffs or barrier island systems characterized by loose, unconsolidated, and easily erodible sediments (Héquette & Barnes 1990; Gibbs et al., 2017). Approximately 80% of the coastline is thought to be erosional (Harper, 1990). Erosion rates on the ABS average between 1-2 m/yr (Reimnitz et al., 1985; Harper et al., 1990, Gibbs et al., 2011) but are locally variable, with maxima of >20 m/yr (Obu et al., 2016). During the open-water season, permafrost-rich coastlines are exposed to both mechanical and thermal erosive energy by means of wave action and direct exposure to warm seawater, respectively (Barnhart et al., 2014). Observed accelerations to Arctic coastal retreat have implications for both sediment supply to the shelf and the adjustment of the nearshore profile, especially given that coastal erosion can occur in the absence of erosion by waves.

Ice processes are an additional mechanism of sediment transport, especially inshore of the 45 m isobath where ice keels can scour and rework seabed sediments (Barnes et al., 1988; Harper et al., 1990). Keel scour occurs within the ”Stamukhi zone,” where landfast ice and pack ice collide and the resulting ice ridges scour the seabed (Reimnitz & Maurer, 1978; Héquette et al., 1995). Bulldozing and scouring of sediments can also occur in the nearshore zone and beach (Barnes & Reimnitz, 1988). However, the majority of ice-driven sediment transport occurs over short distances in the along-shore direction, acting more as an agent of seabed mixing than a control on cross-shelf transport (Hill et al., 1991; Héquette et al., 1995). In winter months, wave and surge development are suppressed, and shorefast and ground ice limit movement of sediments (Manson & Solomon, 2007). Extended periods of stability are sometimes interrupted by events where ice coverage shifts and reworks seabed sediments (Reimnitz et al., 1985).

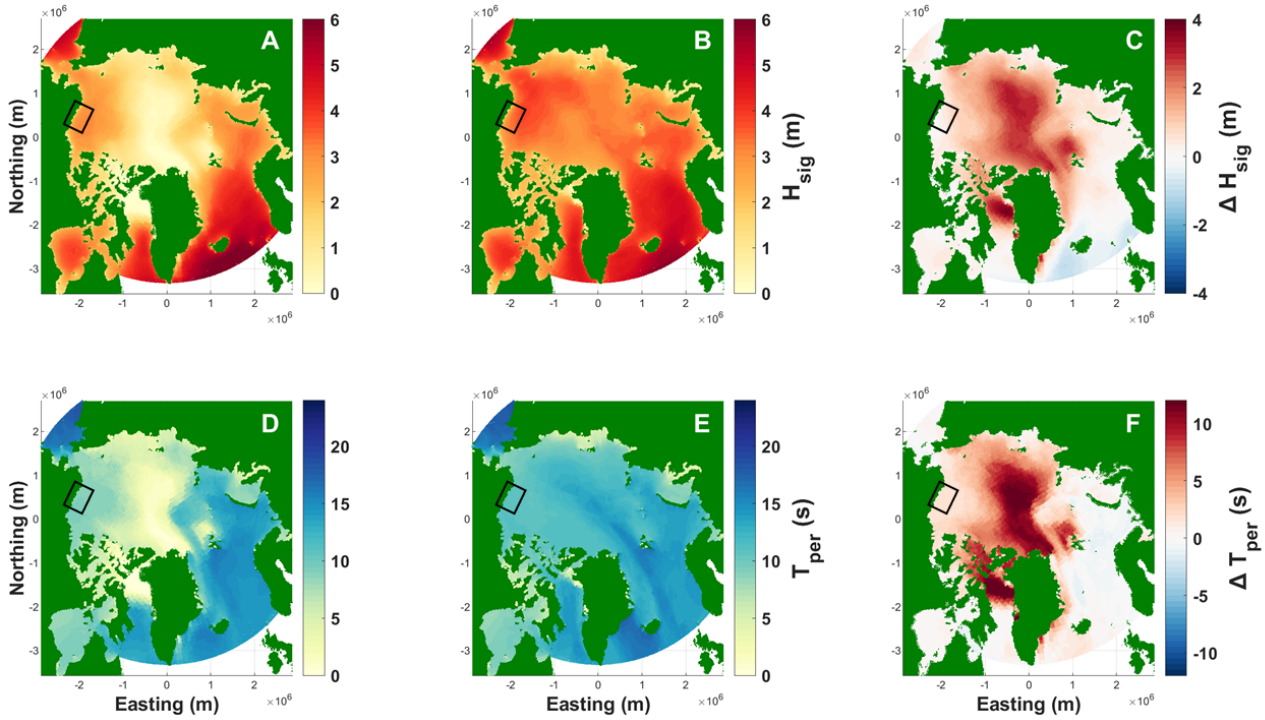

Figure 1.2: Pan-Arctic maps displaying hindcasted present-day (1979-2005) and projected future (2080-2100 under RCP8.5 forcing scenario) wave parameters. Significant wave height (m) shown in panels A and B, with the difference shown in C. Peak wave period (s) shown in panels D and E, with the difference shown in F. These values are averaged over the month of September of each year, the month with the lowest sea ice cover. The ABS is shown by the black rectangle. Data from Casas-Prat et al., (2018).

1.2.2 Arctic Wave Climate

The primary control of Arctic sea states is the presence of sea ice (Hill et al., 1991; Wang et al., 2015; Thomson et al., 2016; Casas-Prat & Wang 2020a). Sea ice exerts control on the sea state through three linked processes: i) fetch-limited wave development; ii) the duration of open-water throughout the year; and iii) the attenuation of waves in the presence of sea ice (Overeem et al., 2011; Thomson & Rogers, 2014). Sea ice extent and duration have declined rapidly over the past several decades, allowing a growth in wave climate. Wave period was observed to increase at a rate of 3-4% per year, and significant wave height increased at a rate of 0.3-0.8% per year between 1970 and 1999 (Wang et al., 2015). Increases in wave height and period are expected to continue into the future (Fig. 1.2) (Casas-Prat & Wang, 2020a). Furthermore, the annual duration of open-water season is presently expanding at a rate of +/- 0.5 days per year (Thomson et al., 2016), leaving Arctic coastlines exposed to erosive forces for a longer period each year (Stroeve et al., 2007; Barnhart et al, 2014). By 2050, the entire Arctic coastline is expected to experience between 60 and 100 additional days of open-water per year as compared to 2016 (Barnhart et al., 2016). The reduction in sea ice and expansion of open-water season allows for higher wave-induced transport capability paired with a longer exposure throughout the year, and is expected to lead to shifts in sediment transport dynamics throughout the Arctic (Barnhart et al., 2014; Casas-Prat Wang 2020b).

1.2.3 Shelf Morphodynamics

Continental shelves are a zone of transition between the deep ocean and the shoreline where wave height attenuation occurs as waves propagate toward the coast. The principal mechanism for sediment transport on a wave-dominated shelf such as the ABS is wave-induced sediment resuspension and subsequent advection by currents, predominantly in the along-shelf direction (Wright, 2012; Dufois et al., 2008; Hill et al., 1991). Though along-shelf sediment fluxes are typically greater in magnitude, cross-shelf sediment fluxes typically have higher gradients, and thus exert a stronger control on the geometry of the shelf profile (Harris & Wiberg, 2002). The cross-shelf gradient in sediment fluxes is due to the depth-dependence of wave-induced bed shear stresses, because wave orbital velocities increase with decreasing water depth. This wave-induced cross-shelf transport of sediment is dependent on the balance between onshore directed asymmetry of wave orbital motions and offshore-directed downslope transport (Ortiz & Ashton, 2016). Fine-grained sediments mobilized by waves can undergo advection via currents or downslope diffusion, and be deposited at greater depths where shear

stresses are relaxed (Harris & Wiberg, 2002; Wright et al., 2012). As a result of the cross-shelf gradient in wave stresses, wave-dominated shelves typically have a concave-upward profile that is maintained in equilibrium at long-timescales by a balance between wave energy dissipation and sediment transport (Friedrichs & Wright, 2004). Thus, the shape of the shelf profile dictates: i) the cross-shelf gradients in wave-driven sediment transport capability; ii) the depths at which erosion and deposition occur; and iii) the distributions of sediment size classes.

The growing Arctic wave climate can be expected to create a state of disequilibrium in which enhanced wave energy alters the present morphodynamic balance. Due to an increased wave climate, mobility of sediments can occur at greater depths across the shelf due to an increase in wave height and deepening of wave base. The ABS has a concave-upward profile with relatively steep inner shelf slopes (1×10^{-3}) transitioning to gentler slopes on the middle shelf (1×10^{-4}). This profile shape is typical of shelves where wave energy is the principal driver of sediment transport because steeper slopes are found on the inner shelf where wave energy dissipation erodes and transports sediments offshore (Fagherazzi & Overeem 2007; Friedrichs & Wright 2004). If the shelf is not in equilibrium as a result of an increased wave climate, the profile may be adjusted by sediment diffusion from areas of higher wave energy dissipation to those with lower wave energy dissipation (Friedrichs & Wright, 2004). However, the morphologic evolution of the shelf can vary from the shortest timescale, the wave orbital motion, to the most extreme and infrequent storms (Nittrouer & Wright, 1994). The long-term evolution of a shelf profile is determined by the sum of short-term adjustment to storm events balanced by recovery during during calmer weather (Anderson et al., 2010, Ogston et al., 2000, Héquette & Hill, 1993). A wave-dominated shelf can be considered in long-term equilibrium when the onshore sediment transport components balance with the offshore component defined by the shelf profile geometry, leading to the maintenance of the shelf profile at centennial to millennial timescales (Ortiz & Ashton, 2016; Dean & Dalrymple, 2004).

In this study the cross-shelf components of shelf sediment transport were isolated from along-shelf components to compare the resultant responses to present-day and projected wave climates. This analysis was conducted for 1000 years to allow the shelf profile to reach a dynamic equilibrium, defined in this context as a shelf profile that maintains its shape through a balance between hydrodynamic and sediment transport phenomena.

1.3 Methods

1.3.1 Model Setup

A 2D cross-shelf sediment transport model was developed using Delft3D-FLOW (Lesser et al., 2004; Roelvink & Walstra, 2003) to evaluate the morphological response of the ABS to a representative present-day and RCP8.5 wave climate. The Delft3D-FLOW module is commonly used for a wide range of coastal engineering and science applications, computing hydrodynamic and sediment transport processes simultaneously as described by Lesser et al., (2004). Sediment transport formulations outlined by van Rijn (2007) were used to calculate bedload and suspended load transport influenced by waves and currents. Wave parameters, significant wave height and peak period were input at the seaward boundary of the model using the SWAN wave computation model coupled with Delft3D-FLOW (Deltares, 2014).

Model experiments were conducted by applying a present-day and RCP8.5 wave climate on a relatively flat (Harrison Bay, AK) and steep (Flaxman Island, AK) ABS bathymetric transect for 1000 years each (Fig. 1.1), allowing shelf morphology to equilibrate to the wave forcing. To reduce computational expense a morphological scaling factor (*MF*) was tested and implemented. Based on the assumption that hydrodynamic and morphodynamic processes are linearly related, bed erosion and deposition are multiplied by *MF* (Lesser et al., 2004; Roelvink & Walstra, 2004). For example, if *MF* = 24, 1 hour of flow computation yields one day of morphologic change (Lesser et al., 2004). A Brier Skill Score (*BSS*) was used to determine the highest *MF* value in which morphologic change could be computed over 1000 years with the minimum computation time, following the methods outlined by Ranasinghe et al. (2011)

$$BSS = 1 - \frac{(z_b - z_{b,mf1})^2}{(z_1 - z_{b,mf1})^2} \tag{1.1}$$

where z_1 is the initial bed slope, z_b is the final bed slope with $MF > 1$, and $z_{b,mf1}$ is the final bed slope for a baseline trial in which *MF* = 10. Present-day waves were applied to the shelf profiles under combinations of flow simulation time and *MF* values (ranging from the baseline value of 10 incrementally up to 500) which represented 1000 years of morphologic change. The results of the sensitivity test showed that a *MF* of 100 can be used to reliably evaluate morphologic change.

To begin the modelling experiments, a morphostatic bed-composition generation (BCG) trial was implemented on each shelf transect for two months to allow for sediment fractionation without vertical bed-level

	Model Parameters	
Location	Harrison Bay, AK	Flaxman Island, AK
Morphology		
Average slope (m/m)	3.0×10^{-4}	8.0×10^{-4}
Non-cohesive d_{50}(μm)	109	80
Cohesive settling velocity (mm/s)	1.0	1.0
Volumetric sand fraction	29	12
Volumetric mud fraction	71	88
Sand porosity	0.40	0.40
Mud porosity	0.60	0.60
Sand critical shear stress τ_c (N/m^2)	0.23	0.23
Mud critical shear stress τ_c (N/m^2)	0.50	0.50
Representative Tides		
Diurnal amplitude (cm)	3.7	6.5
Semidiurnal amplitude (cm)	1.7	2.1

Table 1.1: Initial Delft3D model parameters. Tidal components do not represent total observed tidal amplitudes on the ABS, but instead are isolated diurnal and semidiurnal components used to stabilize the flow field.

change (van der Wegen et al., 2011). Then, the BCG output seabed textures were used as the initial conditions of a 500-year morphodynamic trial under the present-day wave condition. The outputs of this 500 year trial were used as the baseline starting point for the subsequent 1000-year trials analyzed in this paper in order to reduce bias introduced by morphodynamic spin-up and smoothing of bathymetry. Next, sediment transport and shelf morphology were evaluated under two wave climates by conducting 1000-year trials with present-day and RCP8.5 wave conditions on both the Harrison Bay and Flaxman Island shelf transects.

1.3.2 Model Domain

Interactions between shelf geometry and wave propagation were analyzed by using two separate bathymetric transects from the ABS. The ABS at Harrison Bay (Fig. 1.1B) represents a broad and flat shelf section with a slope of 3.0×10^{-4} m/m. In contrast, the shelf section at Flaxman Island (Fig. 1.1C) represents a relatively steep section of the ABS, with a slope of 8.0×10^{-4} m/m. A single regional high-resolution bathymetric product is not presently available. Therefore, bathymetric transects from multiple sources were merged and smoothed from 0 to 80 m depth to create a single representative transect for each profile location. High resolution (25 m) bathymetric data (L. Erickson, personal communication, July 2020) were used for the inner shelf, ship-based 5-cm resolution bathymetric data were used for the middle shelf (J. Thomson, personal communication, March 2020), and International Bathymetric Chart of the Arctic Ocean (IBCAO) (Jakobsson et al., 2020) 200 m

resolution bathymetric data were used for the outer shelf. Landward of the shoreline, a 2-m high bluff/coastal plain was extended 8 km inland to allow for coastal erosion and shelf profile translation. A sigma (σ) coordinate system was implemented in the Delft3D-FLOW domain. For the σ grid, 12 layers of a fixed percentage of the water column are used to represent the vertical dimension. Layer thicknesses were set to be smaller adjacent to the surface and the seabed boundary to improve model stability (Lesser et al., 2004). The cross-shelf horizontal grid resolution increased progressively with depth to adhere to the recommended Courant-Friedrichs-Lewey number for model stability (*CFL*) limit for waves of less than 10 (Lesser et al., 2004; Deltares, 2014)

$$CFL = \frac{\Delta t\sqrt{gd}}{\Delta x} \tag{1.2}$$

where Δt is the timestep duration (s), g is the gravitational constant, d is water depth, and Δx is the grid cell spacing in the cross-shelf dimension. Thus, cross-shelf grid cell lengths were set to 90 m at the coastline, increasing sequentially to 1000 m at the seaward boundary (80 m depth). Thin dams with free-slip walls were added to the sides of the model domain to isolate the cross-shelf components of flow and sediment transport. The offshore boundary condition was an open astronomic boundary and the side boundaries were Neumann time-series boundaries.

Representative seabed textures were implemented for each transect using average fractions and diameters of surficial seabed samples collected *in situ* from cross-shelf transects near Harrison Bay, AK and Flaxman Island, AK. Sediment samples were collected aboard the R/V *Sikuliaq* in fall 2019 and fall 2020 (E. Eidam, personal communication, December 2020) and analyzed for grain-size distributions using a Bettersizer S3Plus laser diffraction sensor. Seabed textures on the ABS are typically patchy and spatially diverse (Barnes et al., 1980). Samples collected in this present study followed this trend, where bimodal matrices of fine sands and fine silts were present with no clear dependence on depth or location.

To construct initial bed compositions in Delft3D-FLOW, sediment populations for both transects were split into their sand ($\geq 63\,\mu\mathrm{m}$) and mud ($< 63\,\mu\mathrm{m}$) populations and the overall transect-averaged grain d_{50} values and fractions were computed for each. Seabed textures implemented in the model are presented in Table 1.1. At Harrison Bay, the representative non-cohesive sand had a d_{50} of $109.7\,\mu\mathrm{m}$, with a volumetric fraction of 29%, accompanied by 71% mud. Flaxman Island was principally composed of a sandy-mud matrix, with an average d_{50} of $80.7\,\mu\mathrm{m}$ and volumetric sand and mud percentages of 12% and 88%, respectively. For cohesive sediments, the Delft3D-FLOW module does not require grain diameter in the sediment transport formulations but rather

requires settling velocity (Deltares, 2014). Thus, settling velocity for the cohesive mud was set to 1 mm/s to represent flocculation of muds in saline environment (Harris & Wiberg, 2002; Sternberg et al., 1999). The initial bed composition for both transects is a uniformly mixed 10 m thick seabed with non-cohesive sediments (sands) and cohesive sediments (muds). The thickness of the top seabed layer, or active layer, was set to 20 cm based on the formulation proposed by Warner et al. (2008):

$$z_a = max[k_1(\tau_{sf} - \bar{\tau_{ce}}\rho_0, 0] + k_2 d_{50} \tag{1.3}$$

where τ_{sf} is the maximum skin friction stress from combined waves and currents, τ_{ce} is the critical shear stress for erosion, ρ_0 is the surface seawater density, d_{50} is the median seabed grain diameter, and k_1 and k_2 are constants 0.007 and 6.0, respectively. Below the top layer, the seabed was split into four layers with thicknesses increasing with depth so that the total seabed thickness was 10 m.

1.3.3 Hydrodynamics

To evaluate the influence of an increased wave climate on the ABS bathymetric sections, two simplified wave climates were applied to the model. The publicly available wave dataset Coupled Model Intercomparison Project Phase 5 (CMIP5) included monthly averaged wave parameters for the entire Arctic over a hindcast period from 1979-2005 and RCP8.5 projected period between 2081 and 2100 (Casas-Prat et al., 2018). The 1979-2005 wave hindcast is hereafter referred to as present-day waves, and the projected 2081-2100 dataset is referred to as RCP8.5 waves. Annual time series for both wave climates were constructed using a weighted monthly averaged wave height and wave period (Fig. 1.3) for the ABS, and repeated at the seaward boundary of the model for the 1000-year duration of the simulations. The weighted monthly average was calculated using a scaling term, q_s, to more adequately capture the enhanced influence of larger waves in determining the equilibrium shelf profile (Ortiz & Ashton, 2016):

$$q_s \propto H_s^5 T_p^{-5} sinh^{-5}(kz) \tag{1.4}$$

where H_s is significant wave height, T_p is peak wave period, *k* is wave number, and *z* is a representative shelf depth at which waves are analyzed. After computing the scaling factor, q_s, the monthly weighted average $\bar{H_s}$ and $\bar{T_p}$ can be calculated as

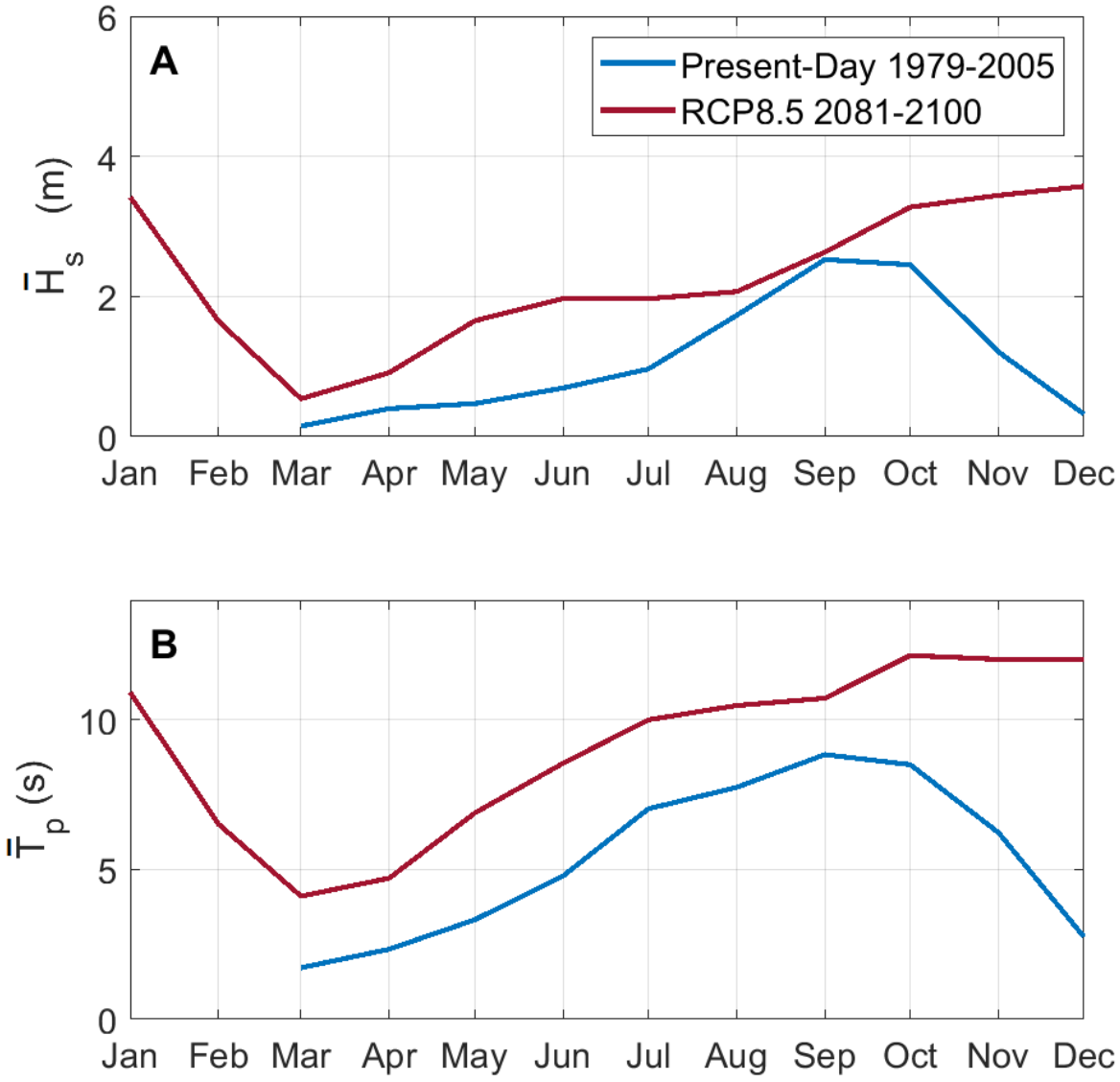

Figure 1.3: Time series of monthly wave parameters $H_s(A)$ and T_p (B) scaled using equation 1.4 implemented in the model. Hindcast shown in blue and projected RCP8.5 waves under climate forcing scenario RCP8.5 shown in red.

Figure 1.4: ERA5 wave hindcast wave parameters (Hersbach et al., 2018), significant wave height (H_s) and peak wave period (T_p), for a storm occurring near the Flaxman Island, AK shelf section between August 23rd and 31st, 2020. This represents a typical ABS storm and was implemented on modelled output shelf profiles.

$$(\bar{H}_s, \bar{T}_p) = \frac{\sum (H_s, T_p) q_s}{\sum q_s} \tag{1.5}$$

where $\bar{H}_s$ and $\bar{T}_p$ are the scaled monthly wave parameters implemented in the model (Fig. 1.3). Furthermore, though ice cover was not included explicitly in the Delft3D-FLOW model, the impacts of reduced ice in the future were represented by stronger waves and a longer open-water season in the RCP8.5 wave climate (Casas-Prat et al., 2018).

Tidal ranges on the ABS are typically less than 20 cm in amplitude and generally produce weak currents less than 3 cm/s near the seabed (Weingartner et al., 2017; Okkonen, 2016). Therefore, simple tides were implemented in the model to stabilize the flow field by extracting the principal diurnal component (M2) amplitude and semidiurnal component (O1) amplitudes and implementing them at the seaward boundary of the model domain (Table 1.1).

1.3.4 Storm Dynamics

To investigate the influence of shelf profile geometry on the delivery of waves to the inner shelf (and resultant potential for sediment transport), a representative 7-day Arctic storm was applied to the 1000-year modelled

shelf sections generated by present-day and RCP8.5 wave climates. Significant wave height and peak wave period time series were implemented at the seaward boundary for each model trial. The storm event lasted approximately 7 days between August 24th to August 31st, 2020. Significant wave heights reached a maximum of 2.5 m with heights above 2 meters sustained over two days. Wave parameters H_{sig} and T_p from the ERA5 wave hindcast model (Hersbach et al., 2018) were retrieved for the duration of the storm on the ABS near the Flaxman Island shelf section (Fig. 1.4).

1.4 Results

Results are presented following the sequence of morphodynamic evolution in the Arctic: a climate-driven growth in wave climate, resultant changes to sediment transport dynamics, morphologic adjustment of the cross-shelf profile, and the feedback between the evolving shelf profile and wave propagation toward the coast.

1.4.1 Long-Term Evolution of Arctic Shelves

1.4.1.1 Waves and Wave-Induced Bed Stresses

A climate-driven growth in wave heights was simulated by conducting model trials in which two different wave climates, present-day and RCP8.5, were imposed at the seaward boundary of the model. The present-day wave climate had an average annual significant wave height (H_s) of 0.91 m, while the RCP8.5 average annual wave height was 2.26 m (Table 2). Average annual wave period (T_p) was 5.05 s in the present-day wave climate and 9.09 s in the RCP8.5 wave climate (Table 2). A change in the duration of the open-water season was represented by imposing present-day waves in which H_s exceeded 0.5 m for 6 months and RCP8.5 waves in which H_s exceeded 0.5 m for 12 months (Fig. 1.3). The contrasting waves were attenuated differently on the two shelves. Wave attenuation was evaluated by calculating the percent decrease in wave heights between the offshore boundary and the 10 m isobath. At Flaxman Island, wave heights attenuated 15% and 23% for present-day and RCP8.5 wave climates, respectively. On the other hand, wave heights at Harrison Bay attenuated 38% and 55% for present-day and RCP8.5 waves, respectively (Table 2). Greater attenuation thus occurred across the wide, shallow, and gently sloping shelf at Harrison Bay, in contrast to the steeper shelf profile at Flaxman Island. Furthermore, H_s averaged across the whole shelf profile revealed that Flaxman Island experienced a 136% increase between present-day and RCP8.5 waves heights as opposed to a 115% increase on the gently sloping

Table 1.2: Wave height and bed shear stress parameters compared between present-day and RCP8.5 wave climates for two shelf sections.

	Harrison Bay		**Flaxman Island**	
Wave Climate	Present-Day	RCP8.5	present-day	RCP8.5
Avg H_s imposed at offshore boundary (m)	0.91	2.26	0.91	2.26
Avg T_p imposed at offshore boundary (p)	5.05	9.09	5.05	9.09
% Difference in H_s between present-day and RCP8.5 waves, from 80 m to 0 m depth	N/A	114	N/A	134
% H_s attenuation between 80 and 10 m depth	37.5	53.7	14.5	23.2
Avg. inner shelf shear stresses, τ_{max} between 25 and 5 m depth (N/m^2)	0.56	1.66	0.97	2.90
Avg. depth of critical shear stress exceedance (m)	31.6	76.0	31.0	73.6
Avg. X-shelf distance of critical shear stress exceedance (km)	89.5	104	23.2	67.0
% Time critical shear stress exceedance for fine sand, 10 m isobath	52	100	50	100
% Time critical shear stress exceedance for fine sand, 40 m isobath	25	67	23	67
Maximum current speed at 25 m depth at 50 cm above bed (cm/s)	3.0	3.1	2.0	2.0

Harrison Bay transect (Table 2). In other words, the same climate-driven increase in wave heights led to a larger increase in wave heights across Flaxman Island than Harrison Bay, due to differences in wave attenuation.

On both transects, wave-induced shear stresses were greater in the RCP8.5 scenario (Fig. 1.5 E & F) because wave orbital velocities scale with the different wave heights imposed. Between 25 m and 5 m depth, average bed shear stresses were greater in the RCP8.5 scenario than in the present-day scenario: 0.56 ± 0.15 N/m^2 (present-day) vs. 1.66 ± 0.07 N/m^2 (RCP8.5) at Harrison Bay and 0.97 ± 0.42 N/m^2 (present-day) vs. 2.90 ± 0.66 N/m^2 (RCP8.5) at Flaxman Island (Table 1.2). Wave-induced bed shear stresses tripled between present-day and RCP8.5 wave climates across both shelves. Bed stresses at Flaxman Island were typically double that of Harrison Bay because less wave attenuation occurred across the steeper transect.

Sediment mobility can be determined by comparing the shear stress exerted on the seabed by fluid motion (wave orbital motion or currents) with the critical shear stress for mobilization of a sediment particle (e.g., van Rijn, 1993). For the fine sands implemented in the modelled seabed, the critical shear stress for mobilization was calculated to be approximately 0.23 N/m^2 for both shelf sections, as the sands had similar median diameters. As a result of increased wave heights, the average depth of critical shear stress exceedance on both shelves was approximately 31 m under present-day waves and 73-76 m under future RCP8.5 waves (Table 2). At Harrison Bay, the shelf break is located at approximately 25 m depth (88 km offshore), and RCP8.5 waves expanded the

envelope of sediment mobilization well beyond the shelf break (Table 2). Despite similar depths of sediment mobilization, critical shear stress exceedance occurred over a broader cross-shelf distance at Harrison Bay than at Flaxman Island (Fig. 1.6). Only 23.2 km of the Flaxman Island transect was within this zone in the present-day wave climate, whereas RCP8.5 waves expanded this zone to 66.9 km (Table 2). Thus, sediment transport was confined to a smaller morphodynamic envelope at Flaxman Island, only extending beyond the shelf break in the RCP8.5 wave climate.

An increased wave climate and lengthened open-water season increased the duration of shear stress exceedance for shelf sediments. The annual percent time of shear stress exceedance on both shelves increased closer to the shoreline, and more than doubled across the entirety of the shelf for the more energetic RCP8.5 wave climate (Fig. 1.6G & 6H). At the 10 m isobath, the duration of critical shear stress exceedance on both shelf sections was approximately 50% per year for present-day waves and 100% per year for RCP8.5 waves. At the 40 m isobath, the duration was approximately 25% per year in present-day waves and 67% per year in RCP8.5 waves. Overall, the mobility of seabed sediment increased as both a function of greater wave height and period as well as a longer duration of exposure to wave orbital motion in an RCP8.5 wave climate.

Tidal forcings were minimal and remained constant in all model trials, and wind forcing was not included. Therefore, the only mechanisms for current-speed evolution through time were changes to water column depth through morphologic adjustment or barotropic flows driven by wave-setup. At Harrison Bay, maximum bottom current speeds measured at the 25 m isobath (50 cm above the seabed) were approximately 3 cm/s for both wave climates. At Flaxman Island, maxima were 2 cm/s at the 25 m isobath.

1.4.1.2 Sediment Transport Response

Wave-induced bed stresses led to greater sediment transport on the narrow and steep Flaxman Island transect than on the broad and flat Harrison Bay transect. Gradients in shear stresses across the shelf were controlled by the decay of wave heights and water depth (Fig. 1.6A & B). As a result, cross-shelf gradients in suspended and bedload transport were dampened across the broad, flat Harrison Bay section and were more substantial on the steep Flaxman Island section (Fig. 1.6C & D).

Overall magnitudes of sediment transport were greater for a) the RCP8.5 wave climate and b) Flaxman Island. We report the cumulative volume of sediment transport after 1000 years totalled across the whole shelf transect. Positive values indicate net onshore-directed transport driven by wave-orbital asymmetry, and negative values indicate downslope transport directed offshore. At Flaxman Island the principle mode of sediment

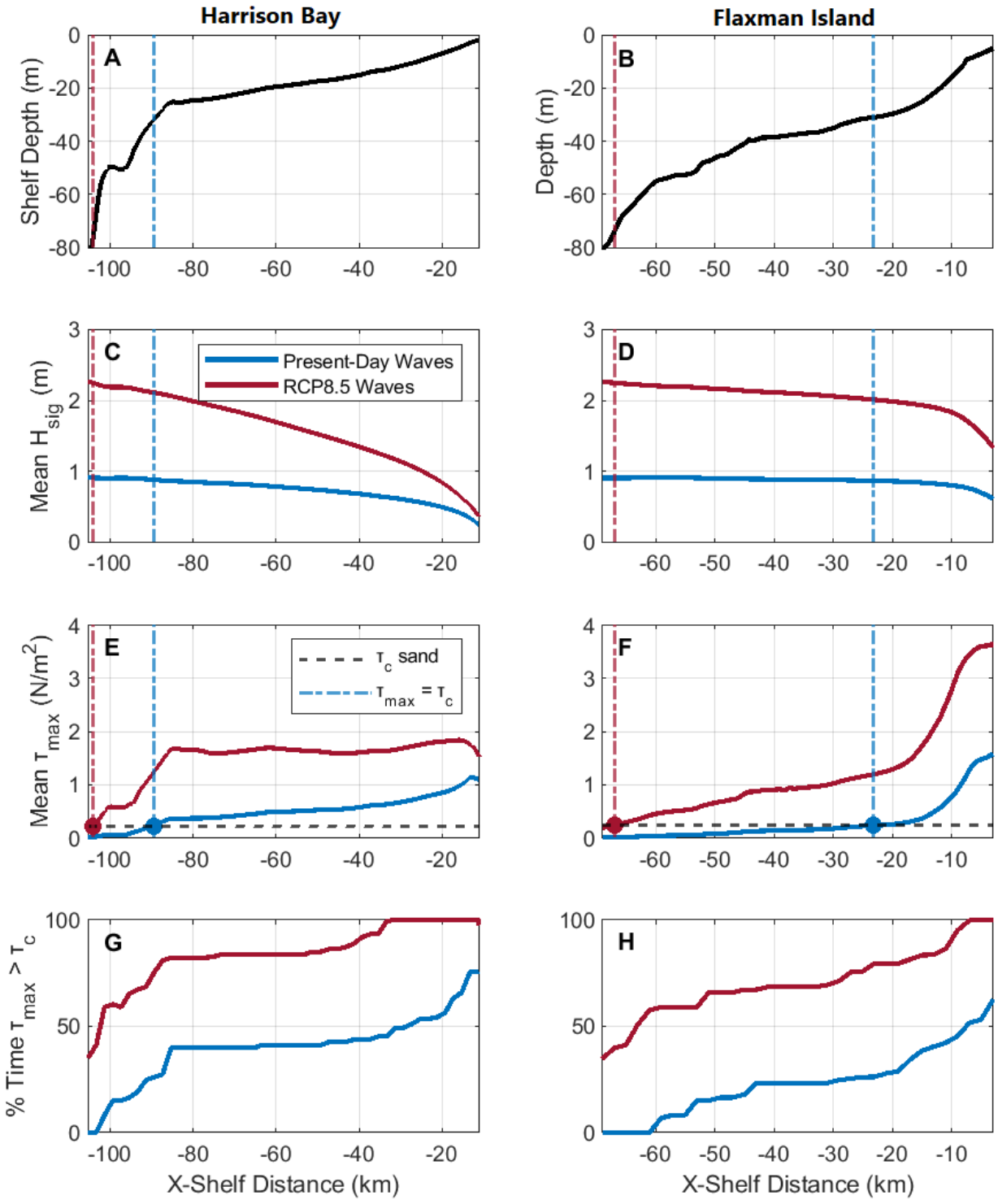

Figure 1.5: Wave heights and wave-induced sediment mobility parameters. Initial cross-shelf sections are shown for Harrison Bay (A) and Flaxman Island (B), along with average cross-shelf wave heights for the present-day and RCP8.5 wave climates (C & D), resultant average wave-induced bed shear stresses are paired with critical shear stress for mobilization (black) of fine sands implemented on each respective shelf section (E & F), and percent duration of 1000 year model run in which critical shear stress for sand is exceeded (G & H). Vertical dashed lines show the outer depth of average sand mobilization in both wave climates.

transport was suspended load, which was two orders of magnitude greater than that of bedload. Suspended load increased by 10-fold from -10.0×10^5 m^3 in the present-day wave climate to -109×10^5 m^3 in the RCP8.5 wave climate (Table 1.3). Suspended sediment transport was prevalent in a distinct morphodynamic envelope, whose seaward boundary expanded from approximately 38 m depth in present-day waves to 71 m depth in RCP8.5 waves (Fig. 1.6D). Bedload transport increased from 0.311×10^5 m^3 in the present-day wave climate to 0.651×10^5 m^3 in the RCP8.5 wave climate, similarly expanding the seaward limit of transport from approximately 17 m depth in present-day waves to 27 m depth in RCP8.5 waves.

Transport at Harrison Bay increased an order of magnitude between the wave climates, from 0.761×10^5 m^3 bedload and 1.99×10^5 m^3 suspended load in the present-day wave climate to 4.16×10^5 m^3 bedload and 30.2×10^5 m^3 suspended load in the RCP8.5 wave climate (Table 1.3). The seaward boundary of onshore-directed bedload transport expanded from approximately 11 m in present-day waves to 40 m in RCP8.5 waves, and suspended load transport occurred in spatially varying zones across the shelf but was greater in RCP8.5 waves (Fig. 1.6C & D).

Opposing directions of suspended load and bedload transport led to a cross-shelf gradient in grain size on the seabed which can provide insight to the fate of eroded sands and muds. On both shelf sections, RCP8.5 waves drove higher magnitudes of change to seabed textures, and sediment fractions changed in opposite ways between the two transects. Initial seabed textures were prescribed as model inputs from observed data. Sand/mud percentages were 29%/71% at Harrison Bay and 12%/88% at Flaxman Island. After 1000 years of exposure to RCP8.5 waves modelled at Harrison Bay, erosion led to winnowing of fines between 60 m and 30 m depth beyond the shelf break, reducing the initial mud fraction to 22% (Table 1.3). Between 0 and 30 m depth winnowing was limited with mud fractions decreasing to 59% in the RCP8.5 wave climate.

In contrast, Flaxman Island experienced winnowing at shallower depths (0 to 30 m depth) and mud accumulation at greater depths (30 to 60 m depths), consistent with the seaward transport of suspended load (Table 1.3). On the inner shelf, winnowing of fines was greater in the RCP8.5 wave climate than in the present-day wave climate, with mud percentages decreasing from 88% initially to 71% and 61% after 1000 years of present-day and RCP8.5 waves, respectively. Mud fractions increased at greater depths from 88% to 94% in both wave climates due to deposition of eroded inner shelf muds (Table 1.3).

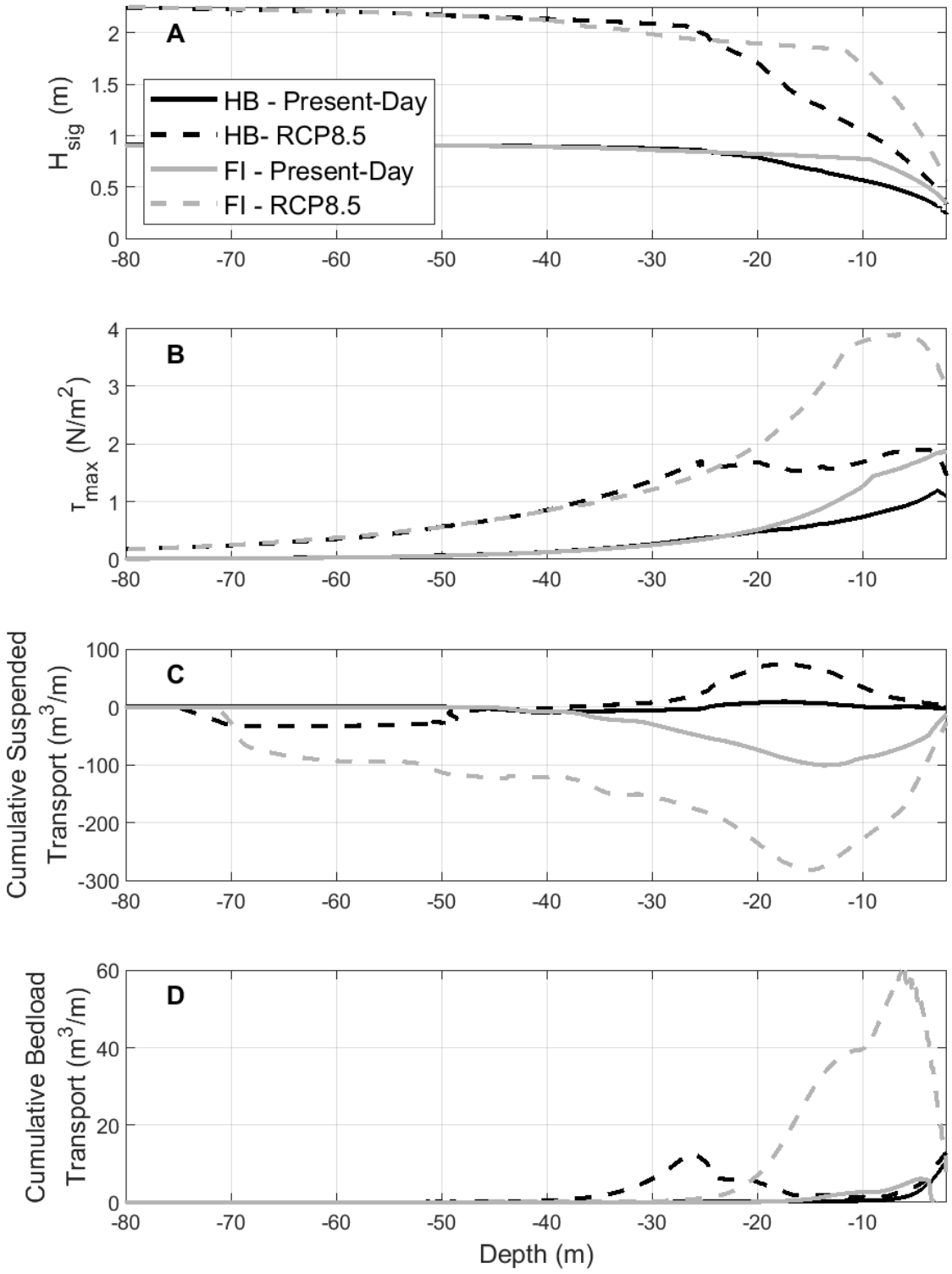

Figure 1.6: Contrasting gradients in sediment transport forcings, average H_s (A) and bed shear stress (B) resulting in contrasting suspended load and bedload transport responses (C and D). Harrison Bay and Flaxman Island are shown as black and gray lines, respectively, and present-day and RCP8.5 waves are solid and dotted lines, respectively.

Table 1.3: Total cumulative sediment transport and final mud fractions between the inner and middle shelves of the four modelled shelf profiles. Negative transport totals indicate seaward sediment transport.

	Harrison Bay		**Flaxman Island**	
Wave Climate	Present-Day	RCP8.5	Present-Day	RCP8.5
Total Volume of Sed. Transport (m^3)				
Bedload	$0.761x10^5$	$4.16x10^5$	$0.311x10^5$	$6.51x10^5$
Suspended load	$1.99x10^5$	$30.2x10^5$	$-10.0x10^5$	$-109x10^5$
Mud Fractions				
Initial fraction	0.71	0.71	0.88	0.88
Final avg. fraction 0 - 30 m depth	0.67	0.59	0.71	0.61
Final avg. fraction 30 - 60 m depth	0.49	0.22	0.94	0.94

1.4.1.3 Morphologic Evolution

The majority of morphologic change occurred at depths shallower than 40 m. The character of morphologic adjustment, i.e., changes to the shelf profile shape, was consistent after 1000 years of exposure to both present-day and RCP8.5 waves. However, the RCP8.5 wave climate drove greater magnitudes of bed elevation changes and slope adjustment.

On both shelves, an inflection point in bed elevation change represented a transition between zones of cross-shelf erosion and deposition. At Harrison Bay, this depth remained static at approximately 17 m for both wave climates, separating an area of slight erosion on the middle shelf from deposition on the inner shelf (Fig. 1.7A & C). This indicates that the shelf profile is static in time and space regardless of wave climate, as landward translation and changes to profile shape are minimal. However, at Flaxman Island the inflection point between inner shelf erosion and middle shelf deposition was 13.6 m in the present-day wave climate and 15.6 m in the RCP8.5 wave climate (Fig. 1.7B & D), indicating that morphologic adjustment occurred to greater depths after exposure to an increased wave climate.

Harrison Bay experienced relatively subtle morphologic changes overall. Erosion occurred near the shelf break, transitioning to deposition on the inner shelf (Fig. 1.7A & C). For the present-day wave climate, an average of 11 cm of erosion occurred around the shelf break (between 40 m and 17 m), in contrast to 3 cm of deposition over a broad distance from 17 m to the shoreline. For the RCP8.5 wave climate, an average of 42 cm of erosion occurred near the shelf break, and 47 cm of deposition between 17 m to the shoreline. Landward transport of sediments resulted in the emergence of an aggradational bar on the 2 m isobath. In addition to relatively minor adjustments to the profile shape, the profile did not undergo landward retreat.

In contrast, Flaxman Island experienced higher morphologic adjustment after exposure to both wave climates where erosion of the shoreline and inner shelf supplied deposition on the middle shelf (Fig. 1.7B & D). After 1000 years of exposure to present-day waves, an average of 1.47 m of erosion occurred between 13.7 m depth and the shoreline. Coastal sediments supplied from the inner shelf were deposited between 13.65 m and 40 m depth, averaging 0.59 m of deposition. The RCP8.5 wave climate yielded bed level changes of the same character as the present-day wave climate, but of a greater magnitude. An average of 3.28 m of erosion occurred on the inner shelf between the shoreline and 15.88 m depth. Deposition on the middle shelf between 15.88 m depth and 40 m depth averaged 0.81 m.

1.4.1.4 Morphodynamic Feedbacks

Notable adjustments to the shelf profile at Flaxman Island enhanced the attenuation of waves propagating to the inner shelf, reducing wave heights at the coast. Decay in wave heights of 5.10% and 7.61% occurred at the 2 m isobaths after 1000 years of exposure to present-day and RCP8.5 waves, respectively (Fig. 1.8B & D). Thus, eroded sediments conveyed to the middle shelf reduced wave heights reaching the inner shelf.

In contrast, wave heights generally remained constant through time at Harrison Bay in the present-day wave climate, with growth in height of up to 1.68% (at the 13 m isobath) and a decay up to 0.71% (at the 7 m isobath) (Fig. 1.8A). In the RCP8.5 wave climate, wave heights grew up to 4.68% at the 13 m isobath where erosion occurred and waves decayed to 3.5% at the 4 m isobath where sediments were deposited on the inner shelf (Fig. 1.8C). As a result of minimal morphologic change, Harrison Bay was relatively insulated from changes to wave heights which limited the potential for a morphodynamic feedback.

1.4.2 Storm Dynamics

Modelled wave heights and resultant shear stresses induced by storm waves were evaluated at the 10 m isobath to explore attenuation of storm waves prior to reaching the inner shelf. Since the same storm was applied to shelf profiles of different shapes, differences in modelled results are attributed to differences in wave attenuation across the shelf.

The delivery of waves to the inner shelf and resultant potential for sediment transport was once again controlled by the existing shelf morphology. Effective attenuation of waves on the flatter Harrison Bay sections led to significant wave heights of 0.60 and 0.61 m at the 10 m isobath on the present-day and RCP8.5 equilibrium shelf profiles, respectively. At Flaxman Island, the same storm generated wave heights of 0.74 m for both

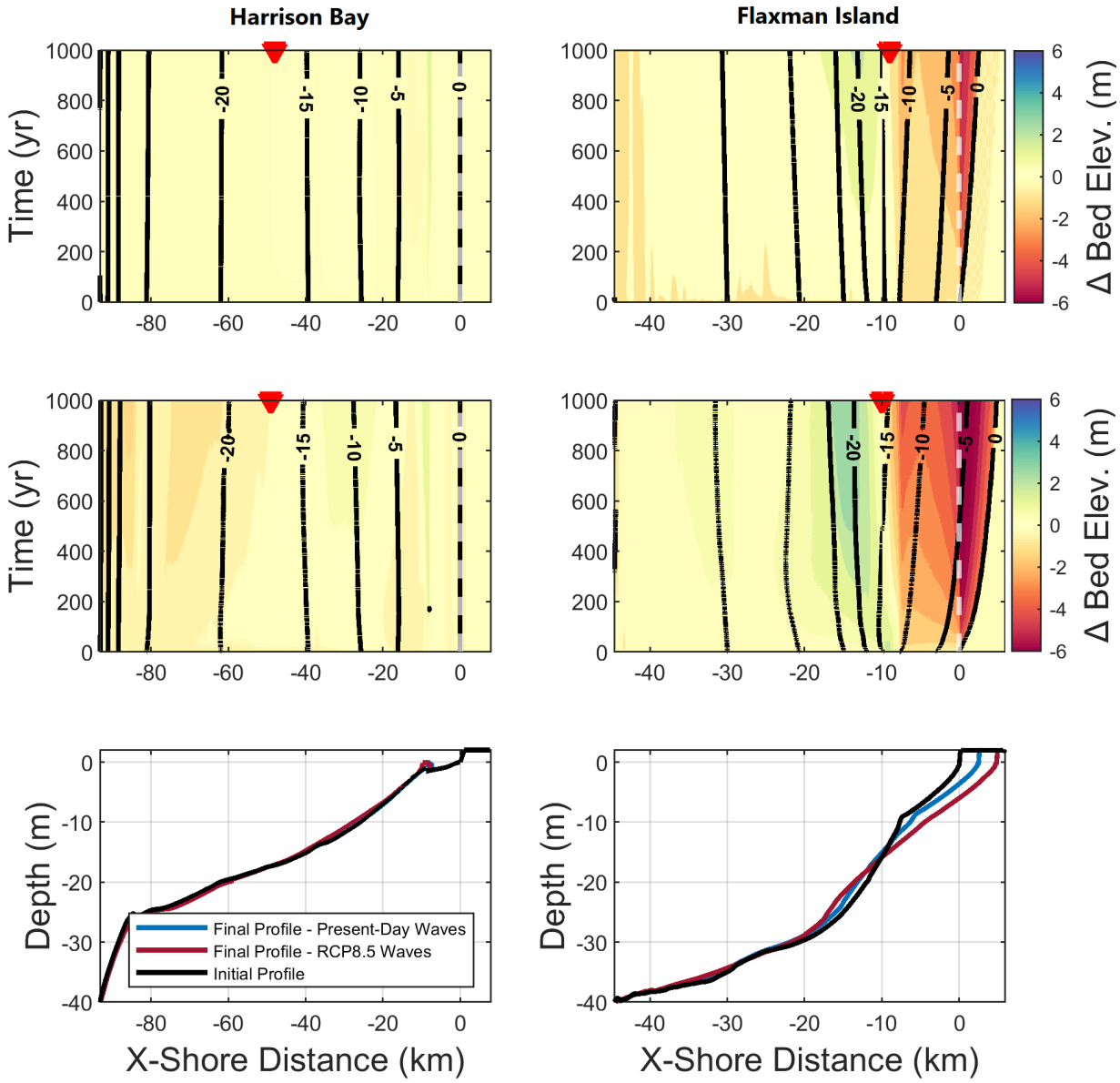

Figure 1.7: Changes in bed elevation through time. Panels A & C show morphologic response of Harrison Bay to present-day and RCP8.5 waves, respectively. Panels B & D show morphologic response of Flaxman Island to present-day and RCP8.5 waves, respectively. Contour lines are shown in black, and initial shoreline positions are shown by the white dashed line. Red triangles are the inflection points between erosion and deposition after 1000 years. Initial and final shelf cross sections are shown for Harrison Bay (E) and Flaxman Island (F).

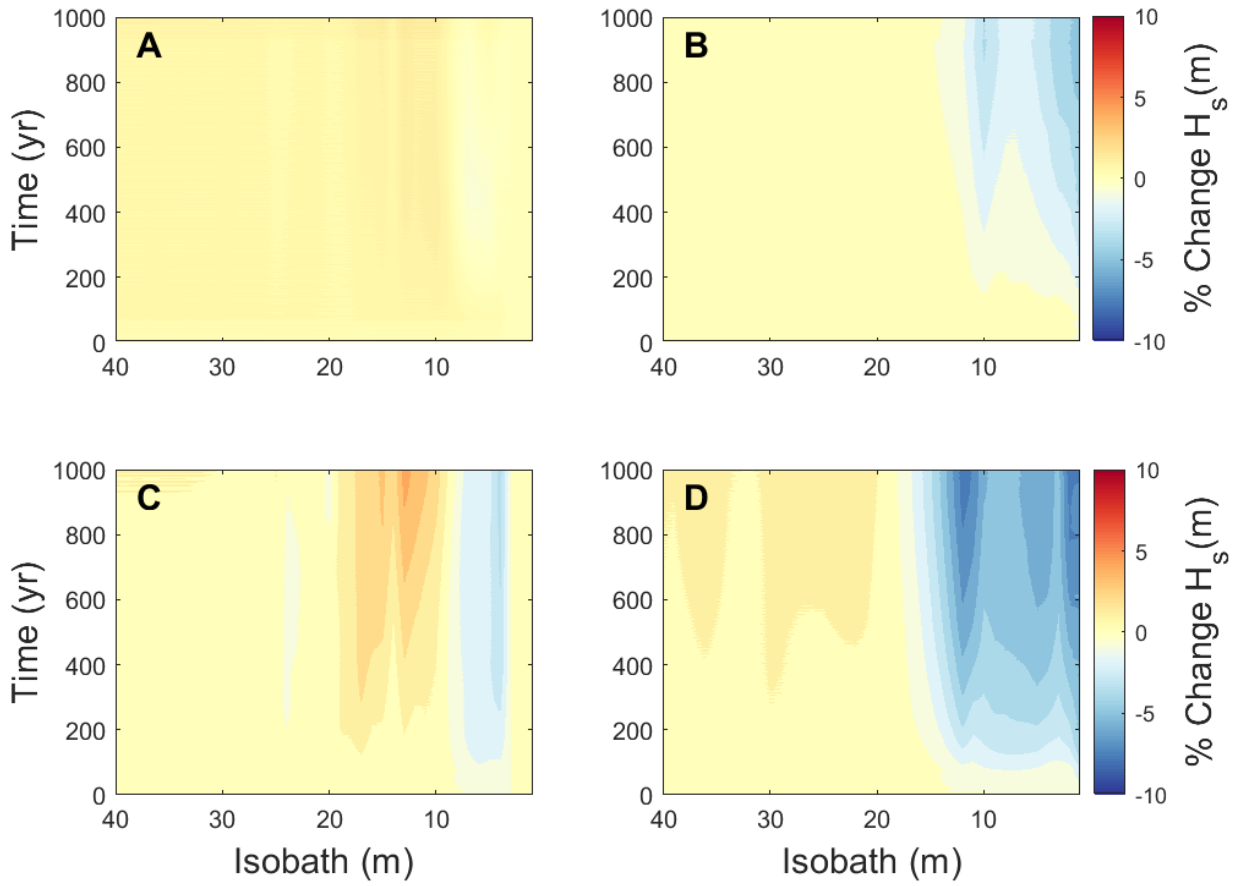

Figure 1.8: Changes in H_s through time driven by morphologic change expressed as a percent change from the initial yearly average. Panels A & C show H_s changes of Harrison Bay to present-day and RCP8.5 waves, respectively. Panels B & D show morphologic response of Flaxman Island to present-day and RCP8.5 waves, respectively.

Table 1.4: Modelled hydrodynamic and sediment transport results from a representative Arctic storm applied to the four output shelf profiles generated in the long-term evolution simulations.

	Harrison Bay		**Flaxman Island**	
Equilibrium Profile	Present-Day	RCP8.5	Present-Day	RCP8.5
Avg. H_s (m) at 10 m depth	0.60	0.61	0.74	0.74
Cum. Wave Power at 10 m depth (kW/m)	8.43×10^6	8.70×10^6	13.9×10^6	13.5×10^6
Avg τ_{max} (N/m^2)	0.85	0.89	1.18	1.16

present-day and RCP8.5 cases (Table 1.4). As a result, the potential for sediment transport on the inner shelf was greater for Flaxman Island. Average bed shear stresses on the 10 m isobath at Flaxman Island were 1.19 and 1.16 N/m^2 on the present-day and RCP8.5-wave equilibrium profiles (Table 1.4). Thus, attenuation of waves passing over the middle and outer shelf exerts a control on the potential for sediment resuspension and transport on the inner shelf.

Wave power on the inner portion of an Arctic shelf has been shown to scale with coastal erosion during storm events (Héquette & Barnes, 1991). Cumulative wave power at the 10 m isobath was calculated in this study using the methods outlined by Defne et al., (2009) and Fenton (1988) where the wave power for a monochromatic wave in shallow water can be computed as a function of significant wave height and mean wave period

$$P(H_s, T_m) = \frac{1}{8}\rho g C_g \tag{1.6}$$

where ρ is water density, g is acceleration due to gravity, and C_g is the velocity of the wave group

$$C_g = \frac{1}{2}\frac{\omega}{k}(1 + \frac{2kh}{sinh(2kh)}) \tag{1.7}$$

where h is the water depth, ω is the angular frequency $\omega = (2*\pi)/T_m$, and k is wavenumber. The broad, gently sloping section at Harrison Bay mitigated the delivery of storm waves to the inner shelf more effectively than the steeper Flaxman Island section. The cumulative wave power at the 10 m isobath at Harrison Bay was 8.43×10^6 (kW/m) and 8.70×10^6 (kW/m) for the present-day and RCP8.5 equilibrium shelf profiles, respectively. At Flaxman Island, the same storm produced a cumulative wave power of 13.9×10^6 (kW/m) and 13.5×10^6 (kW/m) for the present-day and RCP8.5 equilibrium shelf profiles, respectively (values nearly twice that of Harrison Bay, Table 1.4). As shown in Figure 1.9, wave power at Harrison Bay was consistently subdued relative to the Flaxman Island section as a result of the attenuation of peak storm waves prior to reaching the inner shelf. Furthermore, the Flaxman Island section evolved under RCP8.5 waves was shown to be slightly more insulated from storm waves than the present-day Flaxman Island section (Table 1.4) because the middle shelf had shallower depths and thus attenuated waves more effectively.

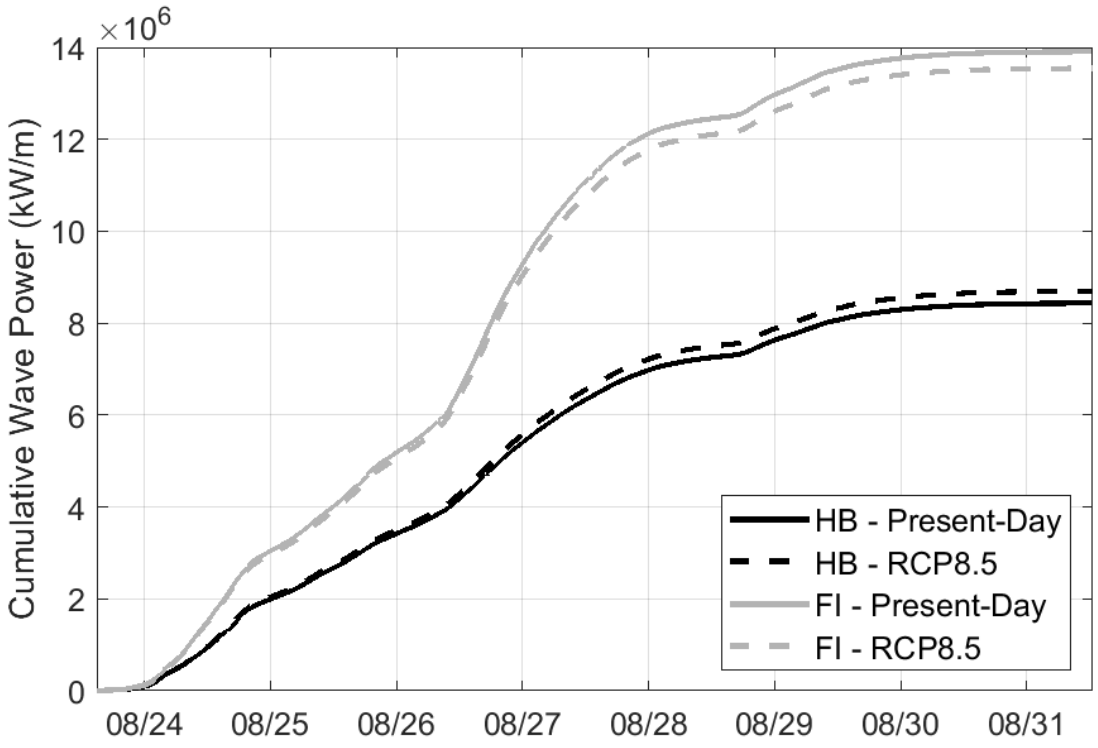

Figure 1.9: Cumulative wave power through the duration of the Arctic storm applied to the Harrison Bay (HB) and Flaxman Island (FI) equilibrium shelf profiles for current (solid) and future (dotted), computed at the 10 m isobath.

1.5 Discussion

As the influence of sea ice on Arctic shelf processes decreases under a warming climate, sediment transport will become increasingly dominated by open-water processes typical of temperate shelves. A projected expansion in fetch due to reduced sea ice is expected to generate a more intense wave climate, and thus greater shear stresses on the seabed. These changes should drive morphologic adjustment of Arctic continental shelves and establish a new dynamic equilibrium. The results of this modelling study demonstrate that relative magnitudes of morphologic adjustment are greater for a) shelves of steeper slopes and b) a projected future wave climate. A broad, gently sloping shelf (Harrison Bay) was relatively insulated from morphologic adjustment in both present-day and RCP8.5 wave climates due to effective cross-shelf attenuation of waves. In contrast, a narrower and steeper shelf (Flaxman Island) was more sensitive to enhanced wave heights and resultant bed shear stresses, which led to greater magnitudes of morphologic change. Furthermore, re-distribution of sediments from the inner shelf to the middle shelf created a feedback between morphologic change and wave attenuation, regulating climate-driven increases to wave heights on a relatively steep shelf.

1.5.1 Wave Attenuation in a Growing Wave Climate

Sea states in the Arctic are presently fetch-limited, both by ocean basin shape and the presence of pack ice (Casas-Prat & Wang, 2020a). The resultant sea state during the open-water season is comparable in magnitude to the Gulf of Mexico (Stopa et al., 2016), but is expected to intensify (Thomson et al., 2016; Casas-Prat & Wang, 2020a). Larger waves will interact with the seabed to greater depths, increasing the zone of potential sediment transport and the cross-shelf distance at which bottom friction can act to dissipate waves (e.g., Pruszak, 2008). As a result, climate-driven increases to the Arctic wave climate can manifest differently on shelves of different geometries. Modelled wave attenuation at Harrison Bay demonstrated that wave base encompassed a broad portion of the shelf, leading to substantial decay of waves propagating toward the coast. Figure 6 (C & D) illustrates the gradual attenuation of both present-day and RCP8.5 waves across long distances at Harrison Bay, in contrast to minimal attenuation of waves across the shelf at Flaxman Island. This is consistent with observations of wave energy dissipation across shelves where bottom friction induced the seabed reduced the energy of waves passing over the shelf (Gon et al., 2020; Ardhuin et al., 2003; Palanques et al., 2002). In the Arctic, shelf sections along the Beaufort, Chukchi, Laptev,and East Siberian seas tend to have broad widths and low relief (Harris et al., 2014), suggesting that effective damping of waves can insulate the inner shelf from both

climate-driven wave growth and resultant morphologic change. Both modelled shelf sections were prescribed the same present-day and RCP8.5 wave climates, but experienced different magnitudes of wave-induced bed shear stresses on the inner shelf due to contrasting wave attenuation across the shelf. For example, between depths of 25 m and 5 m, maximum bed shear stresses averaged over 1000 years of exposure to RCP8.5 waves were 1.66 (N/m^2) at Harrison Bay and 2.90 (N/m^2) at Flaxman Island (Table 2). Thus, the flatter shelf profile was more effective at reducing the impact of the intensified RCP8.5 wave climate on the seabed by attenuating waves across the shelf before they reached shallower depths. Because of this, the potential for wave-driven sediment transport and morphologic response at Harrison Bay was less than for Flaxman Island.

However, the character of morphologic response also depends on whether the changing wave climate is manifest more during extreme storm events or distributed evenly throughout the open-water season (see Ruggiero et al., 2010). In the Arctic, expected wave growth is a result of elongated fetch throughout the year, a dynamic long-term change (Smith & Thomson, 2016), but the expansion of open-water season into the stormy fall season increases exposure to episodic storm waves (Barnhart et al., 2014). This may impact the balance between morphologic disturbances by extreme storm events and fair-weather recovery of the shelf profile (Anderson et al., 2010; Ruggiero et al., 2016; Farquharson et al., 2018), with wave impacts dependent on initial shelf geometry. Thus, long-term predictions for morphologic responses may require a model with a temporal resolution that allows for both the influence of gradual fetch-driven increases to wave heights and increased storm exposure to be considered when projecting changes to the Arctic wave climate.

1.5.2 Morphologic Evolution & Feedbacks

An enhanced wave climate expanded the depth to which sediments were mobilized by waves, broadening the cross-shelf envelope of potential sediment disturbance and morphologic change on both shelves. Notably, morphologic adjustments were minimal at Harrison Bay as the shelf profile remained mostly stable and did not undergo landward retreat, while the Flaxman Island shelf section experienced alterations to the profile shape and retreat. Larger magnitudes and a more pronounced cross-shelf gradient of excess shear stresses on the steeper shelf section (Flaxman Island) led to greater morphologic change to greater depths on the shelf (Fig. 1.5F). After 1000 years of exposure to both present-day and RCP8.5 wave climates, Flaxman Island experienced an average of 1.47 m of erosion on the inner shelf for present-day waves and 3.68 m of erosion for RCP8.5 waves (Fig. 1.8). Sediments eroded by waves from the inner shelf were conveyed downslope to a zone of reduced shear stresses at greater depths, leading to deposition on the middle shelf between 15 and 30 m depth. This redistribution of

sediments accentuated the concave-upward shape of the inner shelf profile. The inflection point between inner shelf erosion and middle shelf deposition also deepened from 13.6 m depth in present-day waves to 15.6 m in the RCP8.5 wave climate, indicating that inner shelf erosion occurred to greater depths and that there was a greater change in shape of the shelf profile through time. On other shelves, stronger waves have been observed to drive sediment transport at greater depths, distributing sediments from zones of erosion on the inner shelf to the middle and outer shelf (Guillen et al., 2006; Diesing et al., 2006; Osbourne & Forest, 2016), consistent with the deepened zones of morphologic change modelled at Flaxman Island under RCP8.5 waves.

Rates of landward translation of the shelf profile also scaled with the input wave climate (Fig. 1.7B & D). This morphologic adjustment to intensified waves was rapid initially but slowed through time, indicating the establishment of a morphodynamic equilibrium shelf profile set by the balance between wave climate, shoreface slope, and sediment textures (Ortiz & Ashton, 2016; Friedrichs & Wright, 2004). Thus, the steeper shelf section was more sensitive to the climate-driven growth in wave climate in terms of wave-induced erosion and landward profile translation, but sensitivity decreased as the shelf profile evolved and stabilized.

In contrast, weak gradients in bed stresses and sediment fluxes on the flat shelf section (Harrison Bay) limited cross-shelf exchange of sediment and resultant morphologic change (Fig. 1.7). Bed level changes across all areas of the shelf were $<$1 m in both wave climates (Fig. 1.8A & C). Since the shape and position of the Harrison Bay profile remained relatively static in time and space under both wave climates, the gently sloping profile was thus in a state of morphodynamic equilibrium.

Redistribution of sediments on the steeper Flaxman Island section led to a regulatory morphodynamic feedback loop. Eroded coastal and inner shelf sediments were deposited in a stress-refuge on the middle shelf, leading to shallowing of the shelf profile and enhanced attenuation of waves propagating to the inner shelf and coast. Wave heights decayed 5.10% and 7.61% at the 2 m isobath as a result of 1000 years of morphologic evolution in the present-day and RCP8.5 wave climates, respectively (Fig. 1.8B & D). This attenuation of waves slowed inner shelf erosion and mitigated the climate-driven increase to waves as the shelf profile evolved. Adjustments to Arctic shelf profiles have the potential to alter the character of waves that propagate to the inner shelf, promoting equilibration of the shelf profile. Furthermore, winnowing of fine-grained sediments in zones of high wave-induced bed stresses on the inner shelf left a surficial layer of coarser sediments that sheltered layers below from the wave boundary layer, armoring the seabed (Wiberg et al., 1994). Since the seabed of the ABS presently has patchy and diverse seabed textures as a result of ice gouging processes (Barnes et al., 1980), reduced sea ice and increased wave energy in the future may result in bed armoring that increases resistance of

the inner shelf seabed to erosion (Harris & Wiberg, 2002; Thieler et al., 1995). This represents another potential mechanism for regulating erosion of inner shelf profiles, because Arctic coasts with coarser sediments have been found to be more resistant to erosion than other coastal morphotypes (Farquharson et al., 2018).

1.5.3 Implications

Arctic continental shelves are a key transition zone in which deep water waves are attenuated as they propagate to the coast. The geometry of the shelf, which can vary in time and space, impacts how a change in wave climate manifests at the adjacent coastline. For example, a low gradient shelf (Harrison Bay) remained insulated from the changing wave climate relative to a higher gradient shelf (Flaxman Island). Wave attenuation across a broad Arctic shelf section like Harrison Bay may mitigate the impacts of wave growth on cross-shelf transport and morphologic adjustment and in turn coastal erosion, while steeper sections like Flaxman Island may have an increased proclivity for wave-induced adjustments to the shape and position of the shelf profile. However, regulatory morphodynamic feedbacks on steeper sections can lead to reduced retreat rates over centennial timescales, indicating that sediment transport processes on steep shelves involve feedbacks which can mitigate the coastal impacts of an increasing wave climate.

Differences in modelled shelf profile evolution also illustrate that there may be a high spatial variability in shelf and coastal evolution in the warming Arctic. These effects will likely be amplified by variability of coastal morphotypes, including shoreface grain size and ice content (Héquette & Barnes, 1990; Farquharson et al., 2018; Harper et al., 1990), which can influence coastal retreat rates and impact long-term shelf evolution via the supply of eroded inner shelf and coastal sediments. On a flat shelf that is relatively insulated from climate-driven growth in wave heights and resultant morphologic adjustment, thermal erosion of permafrost-rich bluffs may be relatively more important than mechanical erosion by waves (Obu et al., 2016). Though the modelled shelf profile of Harrison Bay remained morphologically stable in an intensified wave climate, thermal erosive processes may be the principle mechanism of shoreline retreat. On a steeper shelf profile that is more sensitive to waves, like Flaxman Island, erosion by wave action may continue to intensify in tandem with thermal erosion.

Wave power has been shown to scale with coastal erosion on both Arctic and temperate coastlines, especially during storms (Héquette & Barnes, 1991; Leonardi et al., 2015; Sanford & Gao, 2018). In this study, storm impacts were tested on modelled shelves, and results demonstrated that the cumulative wave power delivered to the inner shelf throughout the storm was strongly controlled by initial shelf geometry. On the steeper shelf

section (Flaxman Island) evolved under RCP8.5 waves, the cumulative wave power delivered to the 10 m isobath was 13.9×10^6 (kW/m). On the flatter shelf section (Harrison Bay) evolved under RCP8.5 waves, only 8.43×10^6 (kW/m) of wave power was delivered to the 10 m isobath during the same storm, a result of effective wave attenuation. Since peak storm waves were found to be attenuated effectively at Harrison Bay but not at Flaxman Island (Fig. 1.9 & 1.10), the impacts of storms may be especially important on steeper, narrower shelf sections.

The findings of this study address key components of the quickly evolving Arctic shelf system: the climate-driven increase in waves, the cross-shelf dimension of sediment transport, and the morphodynamic responses of different shelves. Several Arctic shelf processes can also impact the evolution of the system in a warming climate. In a three-dimensional view, along-shelf fluxes are typically an order of magnitude higher than cross-shelf fluxes but have weaker gradients that reduce their relative impact on morphologic evolution (Palanques et al., 2002; Harris & Wiberg, 2002). On the ABS, model results suggest that broad, shallow Arctic shelves (like Harrison Bay) have a proclivity for wave-driven sediment mobilization in a future wave climate but reduced potential for cross-shelf transport due to low relief. Because of this, gradients in along-shelf transport may be relatively more important than cross-shelf transport on this shelf section given a bimodal, alongshore oriented wind-current regime (Weingartner et al., 2009) paired with high wave-induced bed shear stresses.

In addition to accelerating coastal erosion, riverine sediment supply in the Arctic is expected to increase (Syvitski & Overeem, 2010), adding to the supply of sediments in the shallow shelf environment that can potentially impact the morphologic equilibrium of the shelf profile (Fagherazzi & Overeem, 2007; Friedrichs & Wright 2004). Furthermore, the emergence of an increased Arctic wave climate may vary in space and time, impacting coastal evolution unevenly. Sea level rise on the Beaufort Sea may also impact sediment dynamics. The present rate is approximately 3.5 ± 1 mm/yr and expected to increase (Erickson et al., 2020; Couture et al., 2017) in tandem with the evolving wave climate. But changes to significant wave height in the Arctic are on the order of cm/yr (Wang et al., 2015; Casas-Prat & Wang 2020a), highlighting the importance of the wave climate in the long-term evolution of coastal systems (Ruggiero et al., 2013). Lastly, coastal processes are also complicated by seasonal shorefast ice (Hošeková et al., 2020; Overeem et al., 2011) and barrier islands (Gibbs et al., 2017) which can limit wave power conveyance and resultant sediment transport on the coast. To fully address the implications of climate change on dynamic Arctic shelf systems, high-resolution observational and modelling datasets are necessary to improve projections of how Arctic shelves and coastlines may evolve in the next several centuries.

1.6 Conclusion

This study considered the potential impacts of climate-driven wave growth on the morphology of the Alaskan Beaufort Shelf, and morphodynamic feedbacks which may regulate wave energy reaching the coast. These findings are relevant for the long-term vulnerability of coastal communities and infrastructure across the Arctic due to coastal erosion and changes to the marine environment. In this study we demonstrate the importance of shelf morphology at depths beyond the inner shelf on modifying waves propagating towards the coast.

By developing a sediment transport model representing observed Arctic shelf environments we found that the morphologic response to a growing wave climate was controlled by initial shelf slope geometry. On a steeper shelf transect (Flaxman Island), RCP8.5 waves led to enhanced cross-shelf gradients in wave-induced bed stresses and sediment fluxes. Morphologic change was characterized by distinct zones of erosion on the inner shelf (between 0 and 16 m depth) averaging 3.28 m and deposition on the middle shelf (between 16 and 30 m depth) averaging 0.81 m, as sediments supplied by the eroding inner shelf profile were transported downslope to a zone of relaxed bed shear stresses. Deposition on the middle shelf led to effective dissipation of waves through time, ultimately reducing the height of waves reaching the 2 m isobath by 7.61% over 1000 years of morphologic adjustment. This represents a regulatory morphodynamic feedback in which climate-driven wave growth was mitigated by alterations to the shelf profile, particularly by wave attenuation over the shallower middle shelf. Alterations to the shape of the Flaxman Island shelf profile by wave-induced redistribution of sediments was also paired with landward translation of the shelf profile. In contrast, a wide, flat shelf transect (Harrison Bay) was more effective at attenuating waves propagating across the shelf, insulating the inner shelf from both present-day and RCP8.5 waves and limiting morphologic adjustment and preventing landward retreat. Since waves were attenuated over a broader cross-shelf distance on the flatter shelf section, cross-shelf gradients in bed stresses were subdued, limiting cross-shelf transport and morphologic change. Furthermore, we found that shelf slope played a role in mitigating extreme storm waves across the Harrison Bay shelf section, delivering less wave power to the inner shelf than the Flaxman Island section due to effective attenuation of waves.

The findings of this study illustrate the importance of considering shelf profile geometry and sediment transport processes when evaluating morphologic changes to Arctic shelves and shorelines in a warming climate. This framework can provide insight to shelf environments beyond the Arctic, in which a shift in wave climate can drive differing sediment transport and morphologic responses depending on the initial cross-shelf geometry.

1.7 Data Availability

ERA5 wave hindcast data was obtained by the Copernicus Data Hub (https://scihub.copernicus.eu/), supported by the European Space Agency. Wave mooring data from the Alaskan Beaufort Shelf are available from the data repository for the Coastal Ocean Dynamics in the Arctic (CODA) 2019 cruise (https://doi.org/10.7284/908599). Sediment and bathymetric data were also collected aboard the CODA cruises in 2019 (https://doi.org/10.7284/908599) and 2020 (https://doi.Org/10.7284/908921) and provided via personal communication by Emily Eidam.

APPENDIX A: ADDITIONAL MODEL PARAMETERS

Table A.1: Supplemental overview of sediment transport and hydrodynamic model parameters implemented in Delft3D-FLOW

Parameter	Description	Value
Sediment Transport		
Morfac	Morphologic scaling factor accelerates sediment transport calculations	100
ks	Bed roughness height influenced by skin friction and form drag	0.02
AlfaBs	Streamwise bed-gradient factor for bedload transport	1
AlfaBn	Transverse bed-gradient factor for bedload transport	1.5
SUSc	Current-related suspended sediment transport parameter	0.8
SUSw	Wave-related suspended sediment transport parameter	0.2
BEDc	Current-related bedload sediment transport parameter	1
BEDw	Wave-related bedload sediment transport parameter	0.2
Hydrodynamics		
Flam	Wave breaker delay parameter	2
Gamdis	Wave height to water depth ratio imposes wave breaking	0.5
FwFac	Streaming effect in wave boundary layer, typically set to zero	0
Betarol	Slope of wave front	0.03

BIBLIOGRAPHY

Anderson, T. R., Neil Frazer, L., & Fletcher, C. H. (2010). Transient and persistent shoreline change from a storm. *Geophysical Research Letters*, 37(8), 1–5. https://doi.org/10.1029/2009GL042252

Ardhuin, F., O'Reilly, W. C., Herbers, T. H. C., & Jessen, P. F. (2003). Swell transformation across the continental shelf. Part I: Attenuation and directional broadening. *Journal of Physical Oceanography*, 33(9), 1921–1939. https://doi.org/10.1175/1520-0485

Arp, C. D., Jones, B. M., Schmutz, J. A., Urban, F. E., & Jorgenson, M. T. (2010). Two mechanisms of aquatic and terrestrial habitat change along an Alaskan Arctic coastline. *Polar Biology*, 33(12), 1629–1640. https://doi.org/10.1007/s00300-010-0800-5

Barnhart, K. R., Overeem, I., & Anderson, R. S. (2014). The effect of changing sea ice on the physical vulnerability of Arctic coasts. *Cryosphere*, 8(5), 1777–1799. https://doi.org/10.5194/tc-8-1777-2014

Barnhart, K. R., Miller, C. R., Overeem, I., & Kay, J. E. (2016). Mapping the future expansion of Arctic open water. *Nature Climate Change*, 6(3), 280–285. https://doi.org/10.1038/nclimate2848

Barnes, P. W., & Rearic, D. M. (1985). Rates of sediment disruption by sea ice as determined from characteristics of dated ice gouges created since 1975 on the inner shelf of the Beaufort Sea, Alaska. *USGS Open-File Report*, No. 85- 463.

Barnes, P. W., Reimnitz, E., & Ross, R. (1980). Nearshore surficial sediment textures, Beaufort Sea, Alaska. *USGS Open-File Report*, No. 80- 196.

Barnes, P. W., & Reimnitz, E. (1982). Net flow of near-bottom waters on the inner Beaufort Sea shelf as determined from seabed drifters. *USGS Open-File Report*, No. 85- 463.

Blanco-Chao, R., Costa-Casais, M., Cajade-Pascual, D., & Gómez-Rey, G. (2019). Coastal retreat and sedimentation during the last 3000 years. Atlantic coast of NW Spain. *Journal of Marine Science and Engineering*, 7(10). https://doi.org/10.3390/jmse7100331

Box, J. E., Colgan, W. T., Christensen, T. R., Schmidt, N. M., Lund, M., Parmentier, F. J. W., Brown, R., Bhatt, U. S., Euskirchen, E. S., Romanovsky, V. E., Walsh, J. E., Overland, J. E., Wang, M., Corell, R. W., Meier, W. N., Wouters, B., Mernild, S., Mård, J., Pawlak, J., & Olsen, M. S. (2019). Key indicators of Arctic climate change: 1971-2017. *Environmental Research Letters*, 14(4). https://doi.org/10.1088/1748-9326/aafc1b

Casas-Prat, M., Wang, X. L., & Swart, N. (2018). CMIP5-based global wave climate projections including the entire Arctic Ocean. *Ocean Modelling*, 123(April 2017), 66–85. https://doi.org/10.1016/j.- ocemod.2017.12.003

Casas-Prat, M., & Wang, X. L. (2020). Sea Ice Retreat Contributes to Projected Increases in Extreme Arctic Ocean Surface Waves. *Geophysical Research Letters*, 47(15). https://doi.org/10.1029/2020G- L088100

Casas-Prat, M., & Wang, X. L. (2020). Projections of Extreme Ocean Waves in the Arctic and Potential Implications for Coastal Inundation and Erosion. *Journal of Geophysical Research: Oceans*, 125(8). https://doi.org/10.1029/2019JC0157 45

Couture, N. J., Irrgang, A., Pollard, W., Lantuit, H., Fritz, M. (2018). Coastal Erosion of Permafrost Soils Along the Yukon Coastal Plain and Fluxes of Organic Carbon to the Canadian Beaufort Sea. *Journal of Geophysical Research: Biogeosciences*, 123(2), 406–422. https://doi.org/10.1002/2017JG0 04166

Day, J. J., Holland, M. M., & Hodges, K. I. (2018). Seasonal differences in the response of Arctic cyclones to climate change in CESM1. *Climate Dynamics*, 50(9–10), 3885–3903. https://doi.org/10.100- 7/s00382-017-3767-x

Dean, R. G., & Dalrymple, R. A. (2004). Coastal processes with engineering applications. *Cambridge University Press*.

Defne, Z., Haas, K. A., & Fritz, H. M. (2009). Wave power potential along the Atlantic coast of the southeastern USA. *Renewable Energy*, 34(10), 2197–2205. https://doi.org/10.1016/j.renene.2009.02- .019

Deltares (2014), User Manual Delft3D, *Deltares*, Delft, The Netherlands.

Dufois, F., Garreau, P., Le Hir, P., & Forget, P. (2008). Wave- and current-induced bottom shear stress distribution in the Gulf of Lions. *Continental Shelf Research*, 28(15), 1920–1934. https://doi.org/10.1- 016/j.csr.2008.03.028

Erikson, L. H., Gibbs, A. E., Richmond, B. M., Storlazzi, C. D., Jones, B. M., & Ohman, K. A. (2020). Changing Storm Conditions in Response to Projected 21st Century Climate Change and the Potential Impact on an Arctic Barrier Island – Lagoon System — A Pilot Study for Arey Island and Lagoon , Eastern Arctic Alaska. *USGS Open-File Report*, No. 2020-1142.

Fagherazzi, S., & Overeem, I. (2007). Models of Deltaic and Inner Continental Shelf Landform Evolution. *Annual Review of Earth and Planetary Sciences*, 35(1), 685–715. https://doi.org/10.1146/annurev-.earth.35.031306.140128

Farquharson, L. M., Mann, D. H., Swanson, D. K., Jones, B. M., Buzard, R. M., & Jordan, J. W. (2018). Temporal and spatial variability in coastline response to declining sea-ice in northwest Alaska. *Marine Geology*, 404(April), 71–83. https://doi.org/10.1016/j.margeo.2018.07.007

Fenton, J. D. (1988). The numerical solution of steady water wave problems. *Computers and Geosciences*, 14(3), 357–368. https://doi.org/10.1016/0098-3004(88)90066-0

Fischbein, S. A. (1987). Analysis and interpretation of ice-deformed sediments from Harrison Bay, Alaska. *USGS Open-File Report*, No. 87-262.

Forest, A., Osborne, P. D., Curtiss, G., & Lowings, M. G. (2016). Current surges and seabed erosion near the shelf break in the Canadian Beaufort Sea: A response to wind and ice motion stress. *Journal of Marine Systems*, 160, 1–16. https://doi.org/10.1016/j.jmarsys.2016.03.008

Friedrichs, C. T., & Wright, L. D. (2004). Gravity-driven sediment transport on the continental shelf: Implications for equilibrium profiles near river mouths. *Coastal Engineering*, 51(8–9), 795–811. https://doi.org/10.1016/j.coastaleng.2004.07.010

Gibbs, A. E., Harden, E. L., Richmond, B. M., & Erikson, L. H. (2011). Regional shoreline change and coastal erosion hazards in Arctic Alaska. *In Solutions to Coastal Disasters* 2011 (pp. 258-272).

GIBBS, A. E., NOLAN, M., & RICHMOND, B. M. (2015). Evaluating changes to arctic coastal bluffs using repeat aerial photography and structure from-motion elevation models. *In The Proceedings of the Coastal Sediments 2015*. https://doi.org/10.1142/97898146899770080

Gibbs, A. E., & Richmond, B. M. (2017). National Assessment of Shoreline Change — Historical Shoreline Change Along the North Coast of Alaska , U.S. -Canadian Border to Icy Cape. *U.S. Geological Survey Open File Report* 2015 - 1048, 96. https://doi.org/dx.doi.org/10.3133/ofr20151048.

Gon, C. J., MacMahan, J. H., Thornton, E. B., & Denny, M. (2020). Wave Dissipation by Bottom Friction on the Inner Shelf of a Rocky Shore. *Journal of Geophysical Research: Oceans*, 125(10). https://doi.org/10.1029/2019JC015963

Harper, J. R. (1990). Morphology of the Canadian Beaufort Sea coast. *Marine Geology*, 91(1–2), 75–91. https://doi.org/ 10.1016/0025-3227(90)90134-6

Harris, C. K. (2002). Across-shelf sediment transport: Interactions between suspended sediment and bed sediment. *Journal of Geophysical Research*, 107(C1). https://doi.org/ 10.1029/2000jc000634

Harris, P. T., Macmillan-Lawler, M., Rupp, J., & Baker, E. K. (2014). Geomorphology of the oceans. *Marine Geology*, 352, 4–24. https://doi.org/10.1016/j.margeo.2014.01.011

Harris, P. T., & Macmillan-Lawler, M. (2016). Global overview of continental shelf geomorphology based on the SRTM30_PLUS 30-Arc second database. *Coastal Research Library*, 13(December), 169–190. https://doi.org/10.1007/978-3-319-25121-9$_7$

Héquette, A., Desrosiers, M., Hill, P. R., & Forbes, D. L. (2001). The influence of coastal morphology on shoreface sediment transport under storm-combined flows, *Canadian Beaufort Sea. Journal of Coastal Research*, 17(3), 507–516.

Hequette, A., & Barnes, P. W. (1990). Coastal retreat and shoreface profile variations in the Canadian Beaufort Sea. *Marine Geology*, 91(1–2), 113–132. https://doi.org/10.1016/0025-3227(90)90136-8

Héquette, A., Desrosiers, M., & Barnes, P. W. (1995). Sea ice scouring on the inner shelf of the southeastern Canadian Beaufort Sea. *Marine Geology*, 128(3–4), 201–219. https://doi.org/10.1016/0025-3227(95)00095-G

Héquette, A., & Hill, P. R. (1993). Storm-generated currents and offshore sediment transport on a sandy shoreface, Tibjak Beach, Canadian Beaufort Sea. *Marine Geology*, 113(3–4), 283–304. https://doi.org/10.1016/0025-3227(93)90023-O

Hersbach, H., Bell, B., Berrisford, P., Biavati, G., Horányi, A., Muñoz Sabater, J., Nicolas, J., Peubey, C., Radu, R., Rozum, I., Schepers, D., Simmons, A., Soci, C., Dee, D., Thépaut, J-N. (2018): ERA5 hourly data on single levels from 1979 to present. *Copernicus Climate Change Service (C3S) Climate Data Store (CDS)*. (Accessed on 1-DEC-2020), 10.24381/cds.adbb2d47

Hill, P. R., Blasco, S. M., Harper, J. R., & Fissel, D. B. (1991). Sedimentation on the Canadian Beaufort shelf. *Continental Shelf Research*, 11(8-10), 821-842.

Hill, P. R., Hequette, A., & Ruz, M. H. (1993). Holocene sea-level history of the Canadian Beaufort shelf. *Canadian Journal of Earth Sciences*, 30(1), 103–108. https://doi.org/10.1139/e93-009

Hill, P. R., Mudie, P. J., Moran, K., & Blasco, S. M. (1985). A sea-level curve for the Canadian Beaufort shelf. *Canadian Journal of Earth Sciences*, 22(10), 1383–1393. https://doi.org/10.1139/e85-146

Hošeková, L., Malila, M. P., Rogers, W. E., Roach, L. A., Eidam, E., Rainville, L., Kumar, N., & Thomson, J. (2020). Attenuation of Ocean Surface Waves in Pancake and Frazil Sea Ice Along the Coast of the Chukchi Sea. *Journal of Geophysical Research: Oceans*, 125(12). https://doi.org/10.1029/2020J- C016746

Hudak, D. R., & Young, J. M. C. (2002). Storm climatology of the Southern Beaufort sea. Atmosphere - Ocean, 40(2), 145–158. https://doi.org/10.3137/ao.400205

Jakobsson, M., Mayer, L.A., Bringensparr, C. et al. The International Bathymetric Chart of the Arctic Ocean Version 4.0. *Sci Data 7*, 176 (2020). https://doi.org/10.1038/s41597-020-0520-9

Kistler, R., Kalnay, E., Collins, W., Saha, S., White, G., Woollen, J., Chelliah, M., Ebisuzaki, W., Kanamitsu, M., Kousky, V., Van Den Dool, H., Jenne, R., & Fiorino, M. (2001). The NCEP-NCAR 50-year reanalysis: Monthly means CD-ROM and documentation. *Bulletin of the American Meteorological Society*, 82(2), 247–267. https://doi.org/10.1175/1520-0477(2001)082¡0247:TNNYRM¿2.3.- CO;2

Lacy, J. R., & MacVean, L. J. (2016). Wave attenuation in the shallows of San Francisco Bay. *Coastal Engineering*, 114, 159–168. https://doi.org/10.1016/j.coastaleng.2016.03.008

Leonardi, N., Ganju, N. K., & Fagherazzi, S. (2016). A linear relationship between wave power and erosion determines salt-marsh resilience to violent storms and hurricanes. *Proceedings of the National Academy of Sciences of the United States of America*, 113(1), 64–68. https://doi.org/10.1073/pnas.151- 0095112

Lesser, G. R., Roelvink, J. A., van Kester, J. A. T. M., & Stelling, G. S. (2004). Development and validation of a three-dimensional morphological model. Coastal Engineering, 51(8–9), 883–915. https://doi.org/10.1016/j.coastaleng.2004.07.014

Lynch, A. H., Curry, J. A., Brunner, R. D., & Maslanik, J. A. (2004). Toward an integrated assessment of the impacts of extreme wind events on Barrow, Alaska. *Bulletin of the American Meteorological Society*, 85(2). https://doi.org/10.1175/ bams-85-2-209

Manson, G. K., & Solomon, S. M. (2007). Past and future forcing of Beaufort Sea coastal change. *Atmosphere - Ocean*, 45(2), 107–122. https://doi.org/10.3137/ao.450204

Nittrouer, C. A., & Wright, L. D. (1994). Transport of particles across continental shelves. *Reviews of Geophysics*, 32(1), 85–113. https://doi.org/10.1029/93RG02603

Norton, David & Weller, Gunter. (1984). THE BEAUFORT SEA: BACKGROUND, HISTORY, AND PERSPECTIVE. 10.1016/B978-0-12-079030-2.50007-1.

Obu, J., Lantuit, H., Grosse, G., Günther, F., Sachs, T., Helm, V., & Fritz, M. (2017). Coastal erosion and mass wasting along the Canadian Beaufort Sea based on annual airborne LiDAR elevation data. *Geomorphology*, 293, 331–346. https://doi.org/10.1016/j.geomorph.2016.02.014

Ogston, A. S., Cacchione, D. A., Sternberg, R. W., & Kineke, G. C. (2000). Observations of storm and river flood-driven sediment transport on the northern California continental shelf. *Continental Shelf Research*, 20(16), 2141–2162. https://doi.org/10.1016/S0278-4343(00)00065-0

Ogston, A. S., & Sternberg, R. W. (1999). Sediment-transport events on the northern California continental shelf. *Marine Geology*, 154(1–4), 69–82. https://doi.org/10.1016/S0025-3227(98)00104-2

Okkonen, S. (2016). Sea Level Measurements along the Alaskan Chukchi and Beaufort Coasts Principal Investigator Dec ember 2016.

Ortiz, A. C., & Ashton, A. D. (2016). Exploring shoreface dynamics and a mechanistic explanation for a morphodynamic depth of closure. *Journal of Geophysical Research: Earth Surface*, 121(2), 442–464. https://doi.org/10.1002/2015JF003 699

Overeem, I., Anderson, R. S., Wobus, C. W., Clow, G. D., Urban, F. E., & Matell, N. (2011). Sea ice loss enhances wave action at the Arctic coast. *Geophysical Research Letters*, 38(17), 1–6. https://doi.org/10.1029/2011GL048681

Palanques, A., Puig, P., Guillén, J., Jiménez, J., Gracia, V., Sánchez-Arcilla, A., & Madsen, O. (2002). Near-bottom suspended sediment fluxes on the microtidal low-energy Ebro continental shelf (NW Mediterranean). *Continental Shelf Research*, 22(2), 285–303. https://doi.org/10.1016/S0278-4343(01)00058-9

Pickart, R. S., Spall, M. A., & Mathis, J. T. (2013). Dynamics of upwelling in the Alaskan Beaufort Sea and associated shelf-basin fluxes. *Deep-Sea Research Part I: Oceanographic Research Papers*, 76, 35–51. https://doi.org/10.1016/j.dsr. 2013.01.007

Pratson, L. F., Nittrouer, C. A., Wiberg, P. L., Steckler, M. S., Swenson, J. B., Cacchione, D. A., Karson, J. A., Murray, A. B., Wolinsky, M. A., Gerber, T. P., Mullenbach, B. L., Spinelli, G. A., Fulthorpe, C. S., O'grady, D. B., Parker, G., Driscoll, N. W., Burger, R. L., Paola, C., Orange, D. L., … Fedele, J. J. (2009). Seascape Evolution on Clastic Continental Shelves and Slopes. *In Continental Margin Sedimentation*. https://doi.org/10.1002/9781444304398.ch7

Pruszak, Z., Szmytkiewicz, P., Ostrowski, R., Skaja, M., & Szmytkiewicz, M. (2008). Shallow-water wave energy dissipation in a multi-bar coastal zone. *Oceanologia*, 50(1), 43–58. http://www.iopan.gda- .pl/oceanologia/

Rachold, V., Grigoriev, M. N., Are, F. E., Solomon, S., Reimnitz, E., Kassens, H., & Antonow, M. (2000). Coastal erosion vs riverline sediment discharge in the Arctic shelfx seas. *International Journal of Earth Sciences*, 89(3), 450–460. https://doi.org/10.1007/s005310000113

Ranasinghe, R., Swinkels, C., Luijendijk, A., Roelvink, D., Bosboom, J., Stive, M., & Walstra, D. J. (2011). Morphodynamic upscaling with the MORFAC approach: Dependencies and sensitivities. *Coastal Engineering*, 58(8), 806–811. https://doi.org/10.1016/j.coastaleng.2011.03.010

Reimnitz, E., Graves, S. M., & Barnes, P. W. (1985). Beaufort Sea Coastal Erosion, Shoreline Evolution, and Sediment Flux. *U.S. Geological Survey Open File Report*, No: 85-380, 78.

Reimnitz, E., Kempema, E. W., & Barnes, P. W. (1987). Anchor ice, seabed freezing, and sediment dynamics in shallow Arctic seas. *Journal of Geophysical Research: Oceans*, 92(C13), 14671-14678.

Reimnitz, E., & Maurer, D. K. (1978). Stamukhi Shoals of the Arctic: Some Observations from the Beaufort Sea. *US Geological Survey Open-File Report*, No. 78-666.

Reimnitz, E., Toimil, L., & Barnes, P. (1978). Arctic continental shelf morphology related to sea-ice zonation, Beaufort Sea, Alaska. *Marine Geology*, 28(3–4). https://doi.org/10.1016/0025-3227(78)90018-X

Roelvink, J. A., & Walstra, D. J. (2004). Keeping it simple by using complex models. *Advances in Hydro-science and Engineering*, 6, 1-11.

Romero Manrique, D., Corral, S., & Guimarães Pereira, Â. (2018). Climate-related displacements of coastal communities in the Arctic: Engaging traditional knowledge in adaptation strategies and policies. *Environmental Science and Policy*, 85(April), 90–100. https://doi.org/10.1016/j.envsci.2018.04- .007

Ruggiero, P. (2013). Is the Intensifying Wave Climate of the U.S. Pacific Northwest IncreasingFlooding and Erosion Risk Faster Than Sea-Level Rise? *Journal of Waterway, Port, Coastal, and Ocean Engineering*, 139(2), 88–97. https://doi.org/10.1061/(asce)ww.1943-5460.0000172

Ruggiero, P., Buijsman, M., Kaminsky, G. M., & Gelfenbaum, G. (2010). Modeling the effects of wave climate and sediment supply variability on large-scale shoreline change. *Marine Geology*, 273(1–4), 127–140. https://doi.org/10.1016/j. margeo.2010.02.008

Ruggiero, P., Kaminsky, G. M., Gelfenbaum, G., & Cohn, N. (2016). Morphodynamics of prograding beaches: A synthesis of seasonal- to century-scale observations of the Columbia River littoral cell. *Marine Geology*, 376, 51–68. https://doi.org/10.1016/j.margeo.2016.03.012

Sanford, L. P., & Gao, J. (2018). Influences of Wave Climate and Sea Level on Shoreline Erosion Rates in the Maryland Chesapeake Bay. *Estuaries and Coasts*, 41(2018), 19–37. https://doi.org/10.10- 07/s12237-017-0257-7

Sepp, M., & Jaagus, J. (2011). Changes in the activity and tracks of Arctic cyclones. *Climatic Change*, 105(3–4), 577–595. https://doi.org/10.1007/s10584-010-9893-7

Smith, M., & Thomson, J. (2016). Scaling observations of surface waves in the Beaufort Sea. *Elementa*, 2016(1), 1–12. https://doi.org/10.12952/journal.elementa.000097

Sternberg, R. W., Berhane, I., & Ogston, A. S. (1999). Measurement of size and settling velocity of suspended aggregates on the northern California continental shelf. *Marine Geology*, 154(1–4), 43–53.https://doi.org/10.1016/S0025-3227(98)00102-9

Stopa, J. E., Ardhuin, F., & Girard-Ardhuin, F. (2016). Wave climate in the Arctic 1992-2014: Seasonality and trends. *Cryosphere*, 10(4), 1605–1629. https://doi.org/10.5194/tc-10-1605-2016

Stroeve, J., Holland, M. M., Meier, W., Scambos, T., & Serreze, M. (2007). Arctic sea ice decline: Faster than forecast. *Geophysical Research Letters*, 34(9), 1–5. https://doi.org/10.1029/2007GL0297- 03

Sturtevant, P. M., Lestak, L. R., Manley, W. F., & Maslanik, J. A. (2004). Coastal erosion along the Chukchi coast due to an extreme storm event at Barrow, Alaska. *In Arctic Coastal Dynamics, Report of an International Workshop*.

Thieler, E. R., Brill, A. L., Cleary, W. J., Hobbs, C. H., & Gammisch, R. A. (1995). Geology of the Wrightsville Beach, North Carolina shoreface: Implications for the concept of shoreface profile of equilibrium. *Marine Geology*, 126(1–4), 271–287. https://doi.org/10.1016/0025-3227(95)00082-A

Thomson, J., Fan, Y., Stammerjohn, S., Stopa, J., Rogers, W. E., Girard-Ardhuin, F., Ardhuin, F., Shen, H., Perrie, W., Shen, H., Ackley, S., Babanin, A., Liu, Q., Guest, P., Maksym, T., Wadhams, P., Fairall, C., Persson, O., Doble, M., … Bidlot, J. R. (2016). Emerging trends in the sea state of the Beaufort and Chukchi seas. *Ocean Modelling*, 105, 1–12. https://doi.org/10.1016/j.ocemod.2016.02.009

Thomson, J., & Rogers, W. E. (2014). Swell and sea in the emerging Arctic Ocean. *Geophysical Research Letters*, 41(9), 3136–3140. https://doi.org/10.1002/2014GL059983

van der Wegen, M., Dastgheib, A., Jaffe, B. E., & Roelvink, D. (2011). Bed composition generation for morphodynamic modeling: Case study of San Pablo Bay in California, USA. *Ocean Dynamics*, 61(2–3), 173–186. https://doi.org/10.1007/s10236-010-0314-2

van Rijn, L. (1993). Principles of Sediment Transport in Rivers, Estuaries and Coastal Seas. Principles of Sediment Transport in Rivers , *Estuaries and Coastal Seas*, 1–17.

van Rijn, L. C. (2007). Unified View of Sediment Transport by Currents and Waves. III: Graded Beds. *Journal of Hydraulic Engineering*, 133(7), 761–775. https://doi.org/10.1061/(asce)0733-9429(2007)133:7(761)

Wang, X. L., Feng, Y., Swail, V. R., & Cox, A. (2015). Historical changes in the Beaufort-Chukchi-Bering Seas surface winds and waves, 1971-2013. *Journal of Climate*, 28(19), 7457–7469. https://doi- .org/10.1175/JCLI-D-15-0190.1

Warner, J. C., Sherwood, C. R., Signell, R. P., Harris, C. K., & Arango, H. G. (2008). Development of a three-dimensional, regional, coupled wave, current, and sediment-transport model. *Computers and Geosciences*, 34(10), 1284–1306. https://doi.org/10.1016/j.cageo.2008.02.012

Weingartner, T. J., Danielson, S. L., Kasper, J. L., & Okkonen, S. R. (2009). Circulation and water property variations in the nearshore Alaskan Beaufort Sea (1999–2007).

Weingartner, T. J., Danielson, S. L., Potter, R. A., Trefry, J. H., Mahoney, A., Savoie, M., Irvine, C., & Sousa, L. (2017). Circulation and water properties in the landfast ice zone of the Alaskan Beaufort Sea. *Continental Shelf Research*, 148(August), 185–198.https://doi.org/10.1016/j.csr.2017.09.001

Wiberg, P. L., Drake, D. E., & Cacchione, D. A. (1994). Sediment resuspension and bed armoring during high bottom stress events on the northern California inner continental shelf: measurements and predictions. *Continental Shelf Research*, 14(10–11), 1191–1219.https://doi.org/10.1016/0278-4343(94)90034-5

Wright, L. D. (2013). Recent Advances in Understanding Continental Shelf Sediment Transport. *Sediments, Morphology and Sedimentary Processes on Continental Shelves*, 159–172. https://doi.org/10.1- 002/9781118311172 .ch8

Zhang, X., Walsh, J. E., Zhang, J., Bhatt, U. S., & Ikeda, M. (2004). Climatology and interannual variability of Arctic cyclone activity: 1948-2002. *Journal of Climate*, 17(12), 2300–2317. https://doi.org/10.1175/1520-0442(2004)017<2300:CAIVOA>2.0.CO;2